Influence of Oceanic Boundary Conditions in Simulations of Antarctic Climate and Surface Mass Balance Change during the Coming Century

Gerhard Krinner, Bérangère Guicherd, Katia Ox, Christophe Genthon, Olivier Magand

Influence of Oceanic Boundary Conditions in Simulations of Antarctic Climate and Surface Mass Balance Change during the Coming Century

GERHARD KRINNER, BÉRANGÈRE GUICHERD, KATIA OX, CHRISTOPHE GENTHON, AND OLIVIER MAGAND

Laboratoire de Glaciologie et Géophysique de l'Environnement, CNRS, UJF–Grenoble, Saint Martin d'Hères, France

(Manuscript received 20 September 2006, in final form 6 July 2007)

ABSTRACT

This article reports on high-resolution (60 km) atmospheric general circulation model simulations of the Antarctic climate for the periods 1981–2000 and 2081–2100. The analysis focuses on the surface mass balance change, one of the components of the total ice sheet mass balance, and its impact on global eustatic sea level. Contrary to previous simulations, in which the authors directly used sea surface boundary conditions produced by a coupled ocean–atmosphere model for the last decades of both centuries, an anomaly method was applied here in which the present-day simulations use observed sea surface conditions, while the simulations for the end of the twenty-first century use the change in sea surface conditions taken from the coupled simulations superimposed on the present-day observations. It is shown that the use of observed oceanic boundary conditions clearly improves the simulation of the present-day Antarctic climate, compared to model runs using boundary conditions from a coupled climate model. Moreover, although the spatial patterns of the simulated climate change are similar, the two methods yield significantly different estimates of the amplitude of the future climate and surface mass balance change over the Antarctic continent. These differences are of similar magnitude as the intermodel dispersion in the current Intergovernmental Panel on Climate Change (IPCC) exercise: selecting a method for generating boundary conditions for a high-resolution model may be just as important as selecting the climate model itself. Using the anomaly method, the simulated mean surface mass balance change over the grounded ice sheet from 1981–2000 to 2081–2100 is 43-mm water equivalent per year, corresponding to a eustatic sea level decrease of 1.5 mm yr^{-1}. A further result of this work is that future continental-mean surface mass balance changes are dominated by the coastal regions, and that high-resolution models, which better resolve coastal processes, tend to predict stronger precipitation changes than models with lower spatial resolution.

1. Introduction

Paleoclimatic evidence (e.g., Cuffey et al. 1995; EPICA Community Members 2004) as well as simulations of future climate change (Masson-Delmotte et al. 2006) indicate that climate change in polar regions tends to be amplified compared to the global mean climate change. This raises concern about the potential impact of future polar climate change on global sea level via changes in the mass balance of the major ice sheets. Ongoing mass changes of Greenland and Antarctica have been recently evaluated by Zwally et al. (2005), who suggest that the West Antarctic Ice Sheet is currently losing mass, probably because of ice-dynamic responses to long-term climate change and perhaps past decay of adjacent ice shelves, while East Antarctica is gaining mass, maybe due to increasing precipitation in the last century. This yields a combined net Antarctic impact on the global eustatic sea level of +0.08 mm yr^{-1}. Surface mass balance (SMB; defined as precipitation minus sublimation minus runoff) is the component of the total ice sheet mass balance that is most directly affected by atmospheric climate changes. Model estimates of future Antarctic SMB generally suggest an increase in Antarctic SMB, dominated by a general precipitation increase linked to warmer temperatures, which is not offset by a very slight runoff increase (e.g., Thompson and Pollard 1997; Wild et al. 2003; Huybrechts et al. 2004; Krinner et al. 2007).

Detailed studies of climate change, in particular in regions with strong topographical contrasts such as ice sheet margins, require high-resolution information that

Corresponding author address: Gerhard Krinner, Laboratoire de Glaciologie et Géophysique de l'Environnement (CNRS, UJF–Grenoble 1), BP 96, F-38402 Saint Martin d'Hères CEDEX, France.
E-mail: krinner@ujf-grenoble.fr

DOI: 10.1175/2007JCLI1690.1

can be obtained by several downscaling methods (Giorgi and Mearns 1991). One method consists in using a stretched-grid atmospheric general circulation model (AGCM) with high resolution over the region of interest (e.g., Krinner et al. 2007). With such a model, climate change on the regional scale and its link to the global scale can be simulated in a coherent manner, because the atmospheric model remains global, although it is focused on the region of interest. The required boundary conditions that differ between the present and future model runs are then essentially the atmospheric composition (in particular greenhouse gas concentrations) and sea surface conditions (SSC), that is, sea surface temperature (SST) and sea ice concentration (SIC).

There are two basic methods of prescribing present and future sea surface conditions. The first method consists in using directly the SSC simulated by a previous coupled run, interpolated on the new, higher-resolution grid of the AGCM simulations. This approach has been chosen by Krinner et al. (2007) who noted that some biases of the present-day high-resolution atmosphere-only simulation were caused by the use of the coupled model SSC. The advantage of this method is its simplicity. The second method consists of using an anomaly method in which the present-day simulations use observed SSC, while the simulations for the future use the change in sea surface conditions taken from the coupled simulations superimposed on the present-day observations. The idea behind this method is that the use of the simulated climate change signal only would reduce the effect of systematic model biases (de Noblet-Ducoudré et al. 2000). It is indeed often assumed that systematic errors in climate models may partially cancel between simulations of two different climate states (Pan et al. 2001; Sushama et al. 2006), although some systematic biases in simulations of the present climate have been reported to be strengthened in climate change experiments (Wild et al. 1997). However, Pan et al. (2001) suggest that the ratio of simulated climate change to model biases should be taken as a measure of confidence in projected climate changes; if the use of an anomaly method reduces the model bias compared to a climate change experiment in which coupled model SSC are directly used (which is the case here, as will be shown in sections 3 and 4 of this paper), then confidence in the simulated climate change is increased.

"Anomaly" methods are commonly used in climate impact analysis (e.g., Santer 1985; Füssel and van Minnen 2001) and in studies in which models of a particular component of the climate system (e.g., ice sheet or vegetation models) are forced by the output of a coupled climate model (e.g., de Noblet-Ducoudré et al. 2000; Lunt et al. 2004; Charbit et al. 2002). Anomaly forcing of an atmospheric GCM with the output of a coupled ocean–atmosphere climate model belongs to this class of applications. Krinner et al. (2004) applied an anomaly method to treat the oceanic output of a low-resolution climate model of intermediate complexity in order to use these as oceanic boundary conditions in an AGCM paleoclimate study. Using an anomaly method prevents biases in the prescribed SSC for the present, but one has to face several pitfalls, in particular linked to sea ice. For example, contrary to SST in most cases, SIC changes from the coupled model run cannot be simply added to the present-day observed SIC, because the inevitable biases of the coupled model SIC would almost certainly lead to cases in which the constructed future SIC would locally be below 0% or above 100%. If these problems can be solved, this second method appears generally preferable because it is not directly affected by systematic biases of the coupled model (only its climate change signal is used). One might thus expect it to yield a more realistic picture of the present and future regional climate if the climate change signal is not too strongly affected by modern climate biases. In addition, because of the higher ratio between the simulated climate change and the model bias, confidence in the simulated climate change signal will be increased.

Here we apply an anomaly method applied to high-resolution simulations of the Antarctic climate change between the ends of the twentieth and twenty-first centuries. This is, to our knowledge, the first time such an anomaly method is applied to construct oceanic boundary conditions for an atmospheric general circulation model run in a future climate change experiment. Section 2 describes the method. We then discuss the model climatology, which is briefly compared to simulations carried out with prescribed SSC from a coupled model run (section 3). The simulated Antarctic climate change and its consequences on global eustatic sea level are then described in section 4.

2. Method

a. Simulations

We used the LMDZ4 (Laboratoire de Météorologie Dynamique, CNRS Paris) atmospheric general circulation model (Hourdin et al. 2006), which includes several improvements for the simulation of polar climates as suggested by Krinner et al. (1997). The model was run with 19 vertical levels and 144 $\times$ 109 (longitude times latitude) horizontal grid points. These are regularly spaced in longitude and irregularly spaced in latitude. The spacing is such that the meridional gridpoint dis-

tance is about 60 km in the region of interest southward of the polar circle. Because of the convergence of the meridians, the zonal gridpoint distance becomes small near the pole (80 km at the polar circle and below 60 km south of 77°S) in spite of the relatively low number of zonal grid points. This is the same grid as that used by Krinner et al. (2007).

The simulations last 21 yr each: from 1980 to 2000 and from 2080 to 2100. The first year of both simulations was discarded as spinup. The prescribed greenhouse gas concentrations (CO_2, CH4, N2O, CFC11, CFC12) are measured values for the end of the twentieth century and follow the Special Report on Emissions Scenarios (SRES) A1B scenario for the period 2080–2100. In the following, the present-day simulation is referred to as O20 (because it uses observed SSC), and the simulation for the end of the twenty-first century is called A21 (because it uses the anomaly method).

The prescribed SSC contain monthly and interannual variability. For the present-day simulation, we prescribed the SSC used in the 40-yr European Centre for Medium-Range Weather Forecasts (ECMWF) ReAnalysis (ERA-40; Gibson et al. 1996) for the period of interest. The construction of the SSC for the end of the twenty-first century is described in the following subsection.

In this paper, the simulations O20 and A21 are compared to the simulations carried out by Krinner et al. (2007). These latter runs are identical to O20 and A21, but directly use prescribed SSC without interannual variability from a coupled model run and average greenhouse gas concentrations over the respective periods. The simulations of Krinner et al. (2007) are referred to as S20 and S21 [because this is how these simulations were referred to by Krinner et al. (2007), and because these simulations directly use simulated SSC].

b. Constructing future SSC

The climate change signal used to construct the SSC for our model runs come from the L'Institut Pierre-Simon Laplace Coupled Model, version 4 (IPSL CM4; Marti et al. 2005). LMDZ4 is the atmospheric component of IPSL CM4. The climate sensitivity of IPSL CM4 for a doubling of the atmospheric CO_2 concentration from preindustrial values (3.7°C) is situated in the upper part of the range of coupled models of the Intergovernmental Panel on Climate Change (IPCC) Fourth Assessment Report (de F. Forster and Taylor 2006). The Antarctic polar amplification in IPSL CM4 is 16%; that is, temperature change over Antarctica is 16% greater than that of the global mean. This situates the model close to the average of the Fourth Assessment Report models (Masson-Delmotte et al. 2006). For the end of the twentieth century, we used the IPSL CM4 output of the historic 20CM3 run; for the end of the twenty-first century, we used the SRES A1B scenario run.

SST for our future runs are constructed by taking the SST from IPSL CM4 coupled run for the pertinent year i (between 2080 and 2100) and correcting it for the 1981–2000 mean bias of the IPSL CM4 coupled run: $\mathrm{SST}_i = \mathrm{SST}_{\mathrm{IPSL\ CM4},i} - (\mathrm{SST}_{\mathrm{IPSL\ CM4,1981–2000}} - \mathrm{SST}_{\mathrm{ERA,1981–2000}})$. In this way, the interannual SSC variability prescribed in our future simulations is that simulated by the coupled model. The anomaly method could also have been defined such that the interannual variability of SSC would have been that of the observations. There are arguments in favor of (and against) both possible choices; it is not obvious to us that one or the other should be preferable. The interannual variability of the simulated present and future climate, and its link to the interannual variability of prescribed SSC, is analyzed in section 4c. SST is set to −1.8°C in regions where the sea ice concentration (see following paragraph) is above zero.

SIC is much more complicated to treat. As stated before, simple additions as carried out for the SST can easily lead to negative SIC or values above 100%. We require the method for constructing the future SIC to fulfill several criteria:

1) Regional characteristics of the coupled model's climate change signal (e.g., strong reduction in one sector of the Southern Ocean versus slight increase in another sector) have to be reproduced. This is an obvious requirement to fulfill.
2) The fractional change of total hemispheric sea ice extent between 1981–2000 and 2081–2100, as simulated by the coupled model, has to be conserved. The motivation for this criterion is that sea ice is a strictly positive variable, like precipitation. Anomaly methods usually treat such variables with respect to fractional rather than absolute change (Hewitson 2003), in order to prevent negative values (or, in our case, values above 100%) to occur. Temperatures are more usually treated using absolute anomalies. It is noteworthy in this context that it is easy to show that when temperature is expressed in kelvins, an anomaly method based on fractional change yields results that are very close to those obtained using absolute anomalies, as long as the model biases are much smaller than the absolute temperatures expressed in kelvins (which is the case).
3) The interannual variability in the prescribed future SIC should be that of the coupled model run, in order to be coherent with the SST reconstruction.

The method described in the following has been designed as the simplest procedure yielding results compliant with the criteria outlined above.

The polar regions of both hemispheres are divided into 12 sectors of 30° longitudinal extent each. For each hemisphere ($h = 1, 2$), each sector ($s = 1 \ldots 12$), and each month ($m = 1 \ldots 12$), the coupled model 1981–2000 average monthly sea ice extent $e_{20,h,s,m}$ is calculated as the spatially integrated sea ice concentration in the corresponding sector. The same is done for each year $y = 2080 \ldots 2100$ of the twenty-first century coupled model run, yielding sea ice extents $e_{21,h,s,m,y}$. For each sector, a fractional sea ice extent change from the monthly average 1981–2000 conditions to each month of each year of the last decades of the twenty-first century can then be calculated for both hemispheres:

$$f_{h,s,m,y} = \frac{\sum_{\bar{s}=s-1}^{s+1} e_{21,h,\bar{s},m,y}}{\sum_{\bar{s}=s-1}^{s+1} e_{20,h,\bar{s},m,y}}.$$

These fractional changes f contain information about the regional characteristics of the sea ice changes, allowing us to fulfill the criterion 1 described above. As can be seen from the above equation, the fractional change f for a given sector is calculated using the sea ice extents of the given sector itself and of its two neighboring sectors. This smoothing prevents "jumps" in the constructed sea ice concentration at the sector limits. A total hemispheric fractional change is similarly calculated: $F_{h,m,y} = E_{21,h,m,y}/E_{20,h,m}$. This hemispheric value will be used to control the constructed SIC such that the fractional change of total hemispheric sea ice extent is conserved (thus satisfying criterion 2). Using sea ice extent of the individual months for the end of the twenty-first century, but the multiyear monthly mean sea ice extent for the end of the twentieth century, ensures that the interannual variability from the twenty-first century coupled model run is reproduced in the constructed twenty-first century SSC (criterion 3). The sectorial and hemispheric fractional sea ice changes $f_{h,s,m,y}$ and $F_{h,m,y}$ are then applied to the present-day monthly mean observed SIC (average for 1981 to 2000) as described in the following. The present-day multiyear monthly mean observed SIC is first regridded onto the equal-area polar NSIDC EASE grid at 25-km resolution (Armstrong et al. 1997). These sea ice data are then interpolated over the continents using the boundary condition that there is no sea ice equatorward of 55° latitude. The whole Antarctic continent is replaced by sea ice. The sectorial fractional sea ice changes $f_{h,s,m,y}$ are then applied to this extended sea ice map by replacing the sea ice concentration $c_{i,j}$ in each grid cell (indices i, j) by the maximum of all its neighboring (including itself) grid cells if $f_{h,s,m,y} > 1$ (and correspondingly, the minimum if $f_{h,s,m,y} < 1$):

$$c_{i,j}^{n+1} = \max(c_{k,l}^{n}); \quad k \in \{i-1, i, i+1\}; \quad l \in \{j-1, j, j+1\}.$$

It is this procedure that makes necessary the interpolation of the observed sea ice distribution over the continents mentioned above; otherwise, the absence of sea ice over land could lead to spurious large areas of open ocean in the case of a sea ice reduction, for example, around Arctic islands. The procedure is then repeated until the new constructed sectorial sea ice extent $N_{21,h,s,m,y}$ is close to the observed present-day observed extent $O_{h,s,m}$ times the sectorial fractional sea ice change $f_{h,s,m,y}$:

$$\left| \frac{N_{21,h,s,m,y}}{O_{h,s,m} f_{h,s,m,y}} - 1 \right| = a,$$

where a is set equal to 0.002. The iterations are also terminated if the error $\Delta = N_{21,h,s,m,y} - O_{h,s,m} f_{h,s,m,y}$ changes its sign between two successive steps. In this case, the final sea ice distribution is calculated as a weighted mean between these two successive sea ice distributions, with the weighting chosen such that $\Delta = 0$. The same procedure is then applied to this intermediate twenty-first century sea ice distribution on a hemispheric basis in order to ensure that the fractional change of total hemispheric sea ice extent from the coupled model is reproduced.

Figure 1 displays the monthly mean Antarctic sea ice extent in simulations O20, A21, and from the twentieth and twenty-first century IPSL CM4 coupled runs (which were directly used in the simulations S20 and S21). As stated by Krinner et al. (2007), sea ice extent is underestimated in the coupled IPSL CM4 twentieth-century historic run. The relative error of the coupled model with respect to the observed sea ice extent is corrected by the anomaly method, yielding a larger sea ice extent in A21 than in the twenty-first century IPSL CM4 coupled run directly used in S21. The skewed sea ice seasonality simulated by the coupled model (sea ice minimum too long, sea ice maximum too short) is also corrected by the anomaly method.

Figure 2 displays maps of the (a) observed and (b) simulated 1981–2000 sea ice extents, (c) the 2081–2100

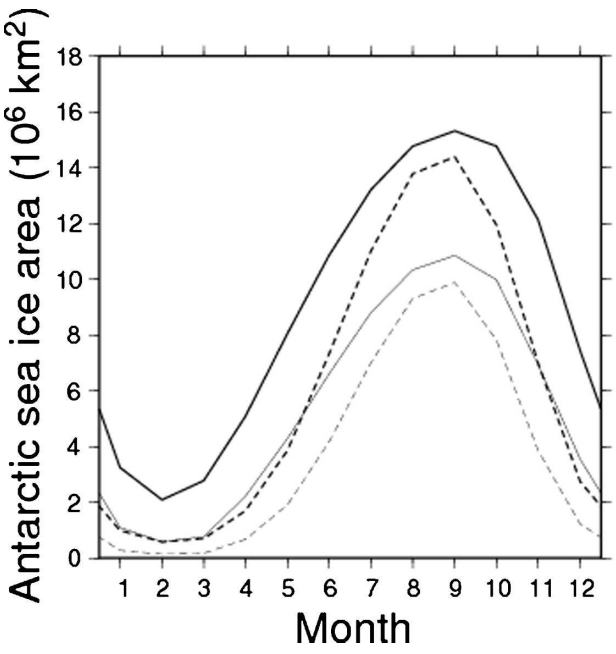

FIG. 1. Prescribed Antarctic sea ice area ($\times 10^6$ km^2): mean values for 1981–2000 and 2081–2100, respectively. Thick continuous line: O20. Thick dashed line: IPSL CM4 coupled run 1981–2000 (used in S20). Thin continuous line: A21. Thin dashed line: IPSL CM4 coupled run 2081–2100 (used in S21).

sea ice extent constructed with the anomaly method, (d) the simulated 2081–2100 sea ice extent, and the sea ice concentration change between the ends of the twentieth and the twenty-first century (e) as constructed using the anomaly method and (f) as simulated by the coupled model. The figure further contains maps of the corrections applied to the simulated (g) twentieth and (h) twenty-first century sea ice concentrations, and (i) the difference between these. One can see that the regional characteristics of the sea ice concentration change simulated by IPSL CM4 (Fig. 2e)—for example, the weak increase off Wilkes Land—are reproduced by the anomaly method (Fig. 2f). Overall, the sea ice concentration change constructed with the anomaly method (Fig. 2f) is stronger than the one simulated by IPSL CM4 (Fig. 2e) because the present-day observed sea ice concentration (Fig. 2a) is higher than the one simulated by IPSL CM4 (Fig. 2b). Nevertheless, the future sea ice extent constructed with the anomaly method (Fig. 2c) remains larger than the one simulated by the coupled model (Fig. 2d), as can also be seen in Fig. 1. Figures 2g and 2h show clearly that the pattern of the differences between S20 and O20 (Fig. 2g) is conserved in the difference between A21 and S21 (Fig. 2h). That is, the spatial pattern of the sea ice concentration bias of S20 is "corrected" in the future climate simulation A21.

3. Model climatology

a. Temperature

Figure 3a displays the annual mean of the absolute monthly surface air temperature bias $\beta = \overline{|T_{\mathrm{obs},i} - T_{\mathrm{mod},i}|}$ ($i = 1 \ldots 12$) (the overline denotes the time mean) in simulation O20. The monthly mean surface air temperature observations used here are Antarctic manned station data compiled by the Scientific Committee on Antarctic Research (SCAR) Reference Antarctic Data for Environmental Research (READER) project (http://www.antarctica.ac.uk/met/READER/) and automatic weather station (AWS) data available via http://uwamrc.ssec.wisc.edu/aws.html. To ensure at least some climatological representativity of the AWS data, their inclusion in this analysis was subject to the conditions that 1) the AWS had to be operational during at least 85% of an individual month and 2) for each month of the year, data had to be available for at least two (not necessarily successive) years. An exception was made for the Dome F AWS, because filtering out data from this AWS would have left a huge data-void region in central East Antarctica. Manned station data were restricted to the period 1981 to 2000, while AWS data were not restricted in time after 2000 in order to allow inclusion of as many AWS as possible (the first AWS were operational at the beginning of the 1980s). The model temperatures were altitude-corrected using the vertical surface air temperature sensitivity to surface altitude changes ($\partial T_s/\partial h_s$) given by Krinner and Genthon (1999). The typical mean error β is about 3° to 4°C. Some strong model errors seem to occur in coastal regions. At least part of these biases are due to the large horizontal climate gradients in the coastal regions. For example, the two data points Dumont d'Urville and D-10 at about 144°E, 67°S are only distant by about 10 km. The Dumont d'Urville research station is situated on an island a few kilometers off the coast, while D-10 is an AWS on the ice sheet a few kilometers inland. Climate differs quite strongly between these two places, which are represented by the same GCM grid point. As a consequence, the model error β (which takes into account an altitude correction, but does not correct for physical characteristics of the observation site, which, in particular at coastal sites, might differ from the large-scale characteristics) is below 1°C for D-10, while it is 4.4°C for Dumont d'Urville. Obviously similar cases might occur at other coastal sites. Another suspect point is the Theresa AWS at 84.6°S, 115.8°W, where β exceeds 6°C. As can be seen in Fig. 2a, the model biases at other data points close to the Theresa AWS are much lower, and there is no obvious reason why

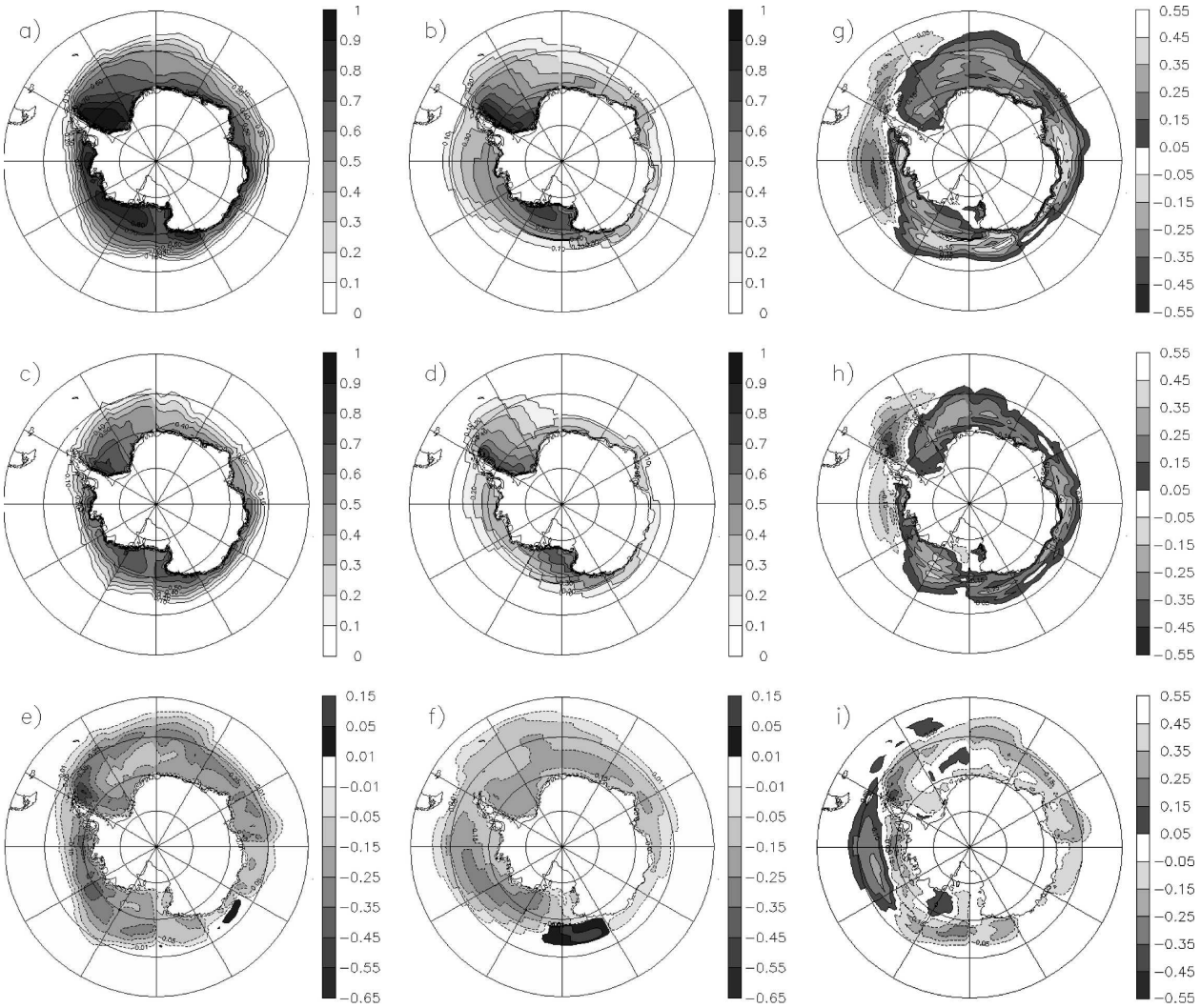

FIG. 2. Annual mean sea ice concentrations (no unit, between 0 and 1) and changes: (a) O20; (b) S20; (c) A21; (d) S21; (e) A21–O20; (f) S21–S20; (g) O20–S20; (h) A21–S21; (i) (A21–S21) − (O20–S20) [=(A21–O20) − (S21–S20)].

the model performance should be locally so bad in a fairly uniform region. We therefore suspect that the Theresa AWS data might be erroneous.

Figure 3b displays the difference in the annual mean of the absolute monthly surface air temperature bias β between O20 and S20. The impact of using observed SSC, compared to (biased) SSC from a coupled model, is not very strong. The use of observed SSC reduces the surface air temperature biases in West Antarctica, but the model performance is slightly deteriorated in East Antarctica. This means that error compensation by biased SSC, which does not occur in O20, misleadingly improves the apparent model performance in S20 in East Antarctica. As expected, using observed SSC improves the model performance particularly in regions with oceanic climate (Southern Ocean islands and the Antarctic Peninsula, especially at the tip).

b. Sea level pressure

Figure 4 displays the simulated sea level pressure in O20 and S20 compared to the ERA-40 data for 1981–2000 for December–February (DJF) and June–August (JJA). At both seasons, a clear reduction in the bias over the Southern Ocean appears in O20 (Figs. 4a,c) compared to S20 (Figs. 4,d). Here the beneficial impact of using observed SSC is obvious. Nevertheless, the spatial structure of the biases is similar in O20 and S20. In winter, the model underestimates the intensity of the Amundsen Sea low (Figs. 4c,d) and shows a ternary negative bias pattern at lower latitudes (40° to 60°S). The summer bias pattern is vaguely reminiscent of the winter pattern, but the biases are weaker, and almost vanish for O20.

It has been shown before that Antarctic sea ice con-

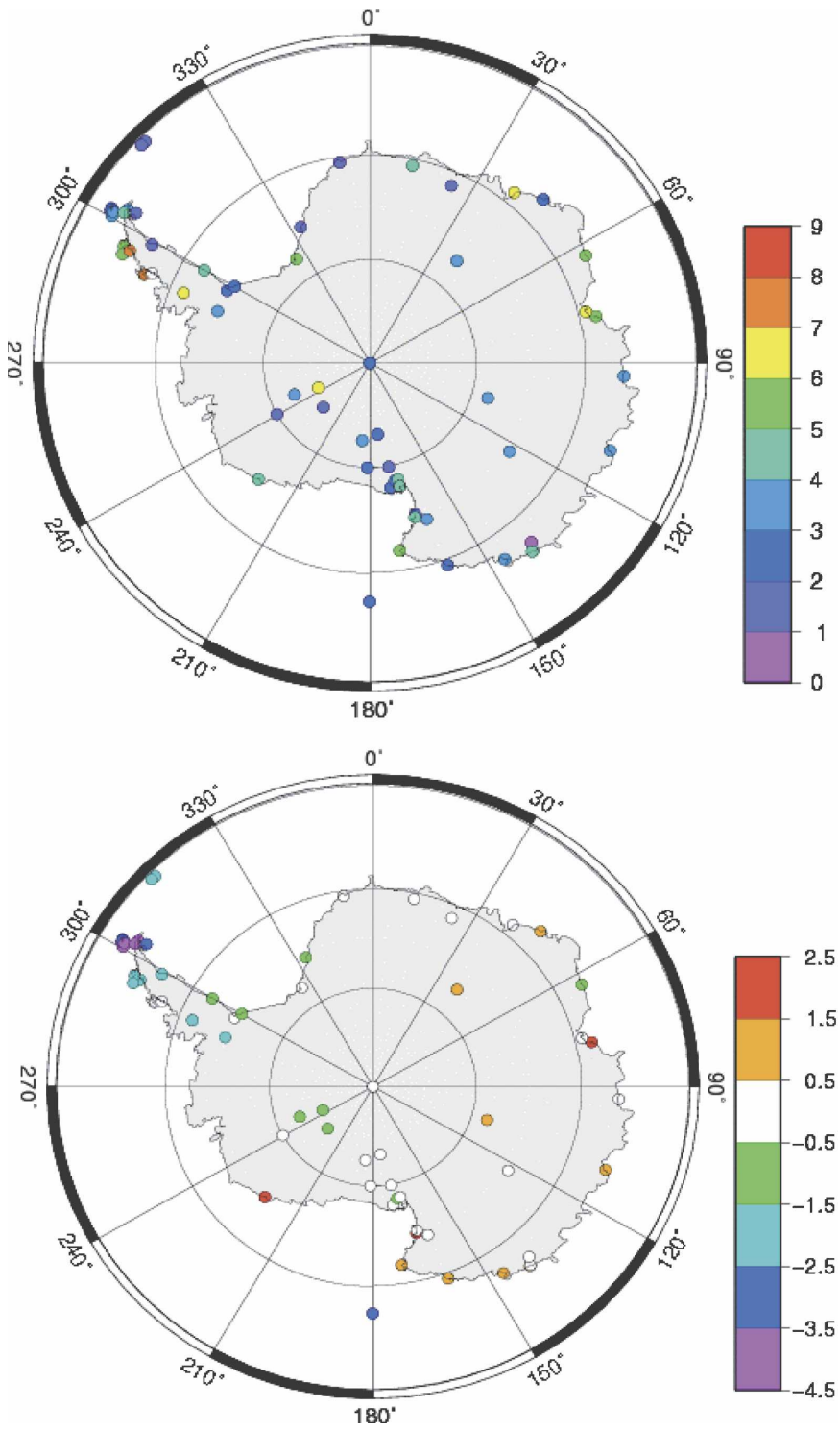

FIG. 3. Simulated surface air temperature compared to AWS and manned station measurements. (a) Mean absolute monthly mean error (see text) in °C for simulation O20. (b) Difference in the mean absolute monthly mean error between O20 and S20.

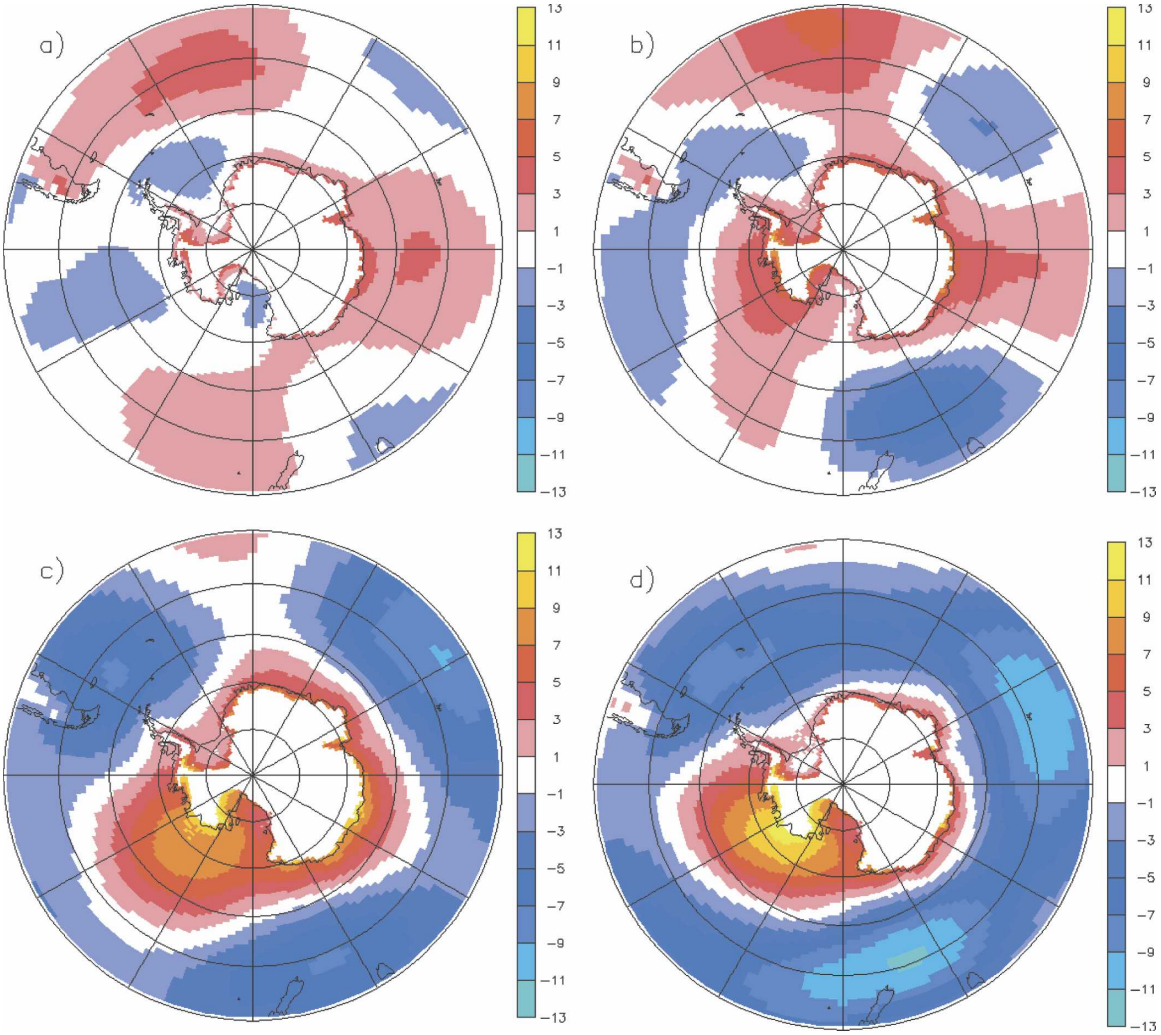

FIG. 4. Bias of the simulated annual mean sea level pressure (hPa) with respect to ERA-40 data for 1981 to 2000: (a) O20 − ERA-40, DJF; (b) S20 − ERA-40, DJF; (c) O20 − ERA-40, JJA; (d) S20 − ERA-40, JJA. Values masked in regions with surface elevation >1000 m.

centrations strongly influence the regional atmospheric circulation (e.g., Simmonds and Budd 1991; Simmonds and Wu 1993). A significant improvement of the simulated sea level pressure patterns in response to using "perfect" oceanic boundary conditions is therefore an expected model behavior.

c. Surface mass balance

Following Krinner et al. (2007), the simulated surface mass balance is defined as $B = S + fR - E - (1 - f)M$, where S is the snowfall, R the rainfall, E the mass flux associated with turbulent latent heat transfer (positive upward), M the melt, and f the fraction of liquid surface water that freezes during percolation in the snowpack (Pfeffer et al. 1991; Thompson and Pollard 1997). This definition neglects transport and sublimation of blowing snow, which can locally be an important component of the surface mass balance (Gallée et al. 2001; Frezzotti et al. 2004).

Krinner and Werner (2003) propose a measure of the skill of climate models in reproducing observed surface mass balance (for positive mass balances only). In this definition, the model skill s is calculated as

$$s = \min\left(\frac{B_{\mathrm{Obs}}}{B_{\mathrm{Mod}}}, \frac{B_{\mathrm{Mod}}}{B_{\mathrm{Obs}}}\right).$$

The calculated skill varies between 0 (large error) and 1 (perfect agreement). Figure 5a shows the surface mass balance skill of simulation O20 for the data points selected by Krinner et al. (2007). The data points were selected for the reliability of the method and the length of the record; see Krinner et al. (2007) and references

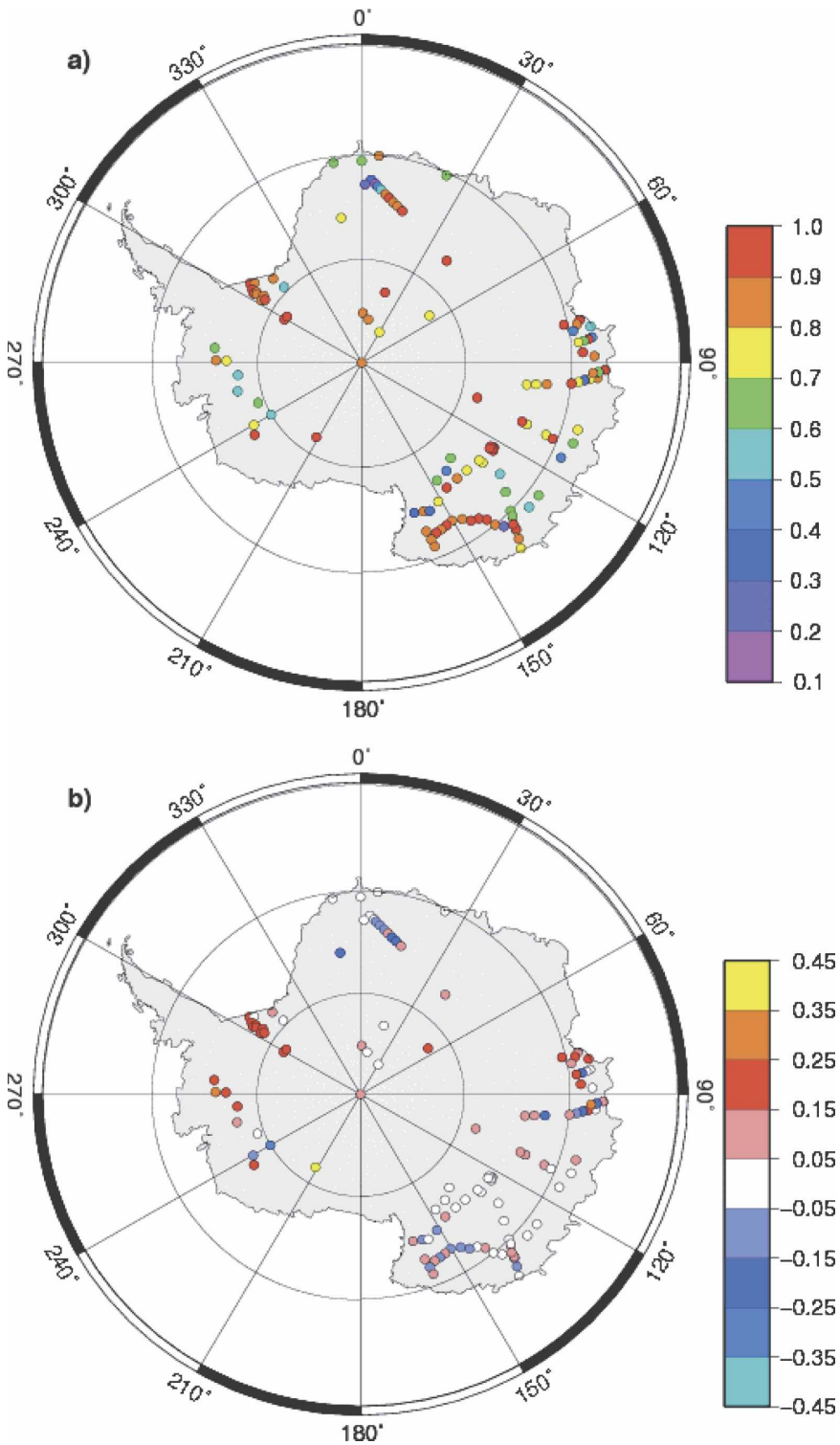

FIG. 5. Surface mass balance skill (between 0 and 1; dimensionless). (a) Simulation O20; (b) difference between O20 and S20.

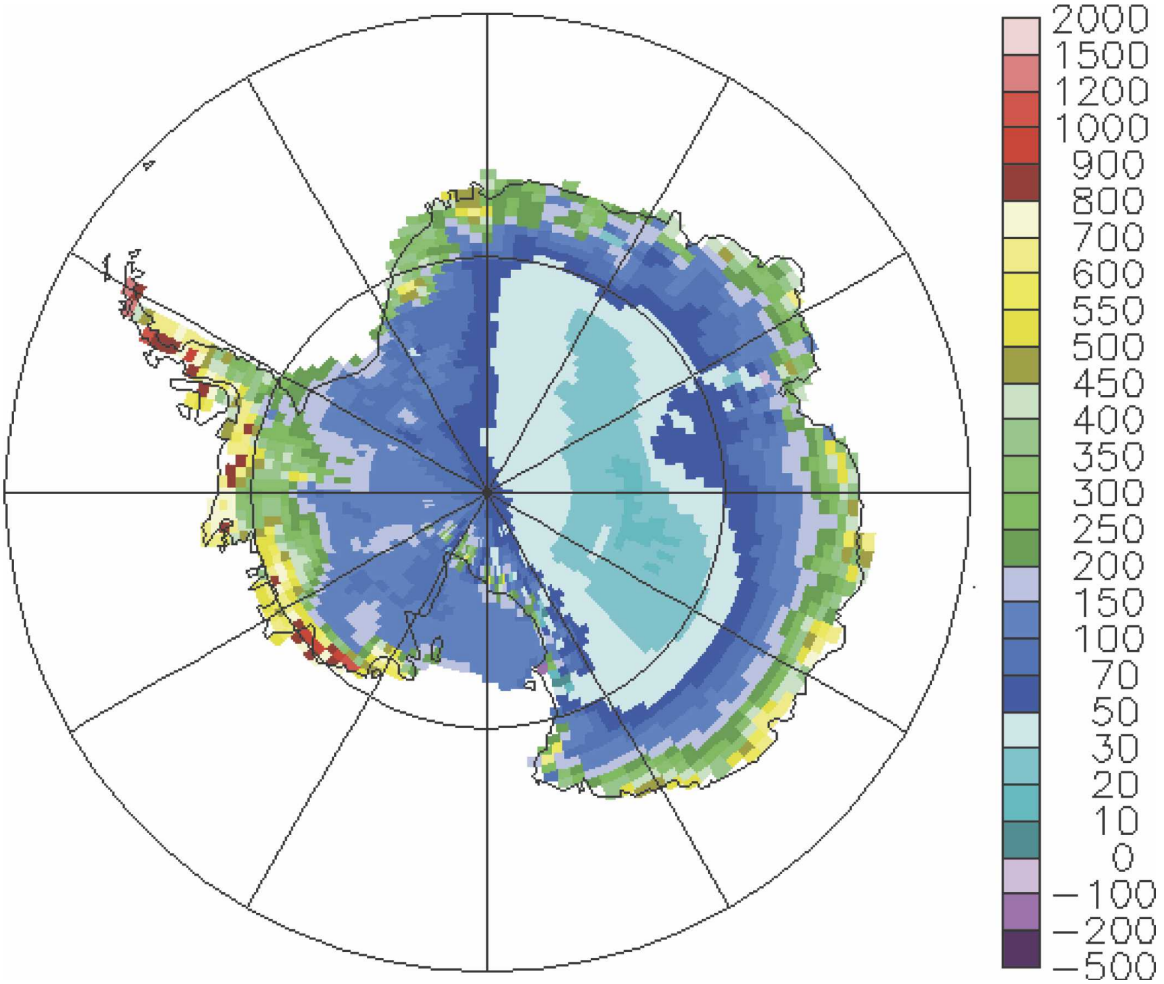

FIG. 6. Surface mass balance (kg m^{-2} yr^{-1}) simulated in O20 for 1981–2000.

therein. The model skill is generally fairly high, the mean value being 0.77, that is, an over- or underestimate of the observed surface mass balance of about 20%. In places where several data points fall into one GCM grid box, the difference between these observational data is typically of the order of 10%. In these cases, even a "perfect" model could therefore not exceed a skill of about 0.95 (5% deviation from each of the individual data points). Taking these 10% as an estimate of the continental average variability at spatial scales unresolved by the GCM, we therefore suggest that 0.95 would be the continental average score of a perfect model, and that the 0.77 obtained by LMDZ4 therefore indicates that the model error is typically below 20%. There are indications that the kilometer-scale SMB variability in Antarctica might actually be much higher, of the order of 30% (Frezzotti et al. 2005; Arthern et al. 2006), further reducing the maximum skill a "perfect" model would obtain.

As stated by Krinner et al. (2007), the simulated surface mass balance is regionally fairly sensitive to biases of the prescribed SSC in S20. This is quantified in Fig. 5b, which displays the skill difference between O20 and S20. This difference is mostly positive, indicating a higher skill in O20 than in S20. Similar to what has been seen for the temperature, the improvements are most notable in West Antarctica, where the influence of the oceanic conditions on the ice sheet climate and its variability is strong (e.g., Genthon et al. 2005).

The continental mean surface mass balance in O20 is 160 kg m^{-2} yr^{-1}, which is not very different from the 151 kg m^{-2} yr^{-1} given by Krinner et al. (2007) for S20. The accumulation, which is also 160 kg m^{-2} yr^{-1} because runoff is negligible, falls within the range of observational estimates between 135 and 184 kg m^{-2} yr^{-1} (Giovinetto et al. 1992; Yamazaki 1994). Figure 6 displays the annual mean surface mass balance simulated in O20. It shows the well-known pattern of very low

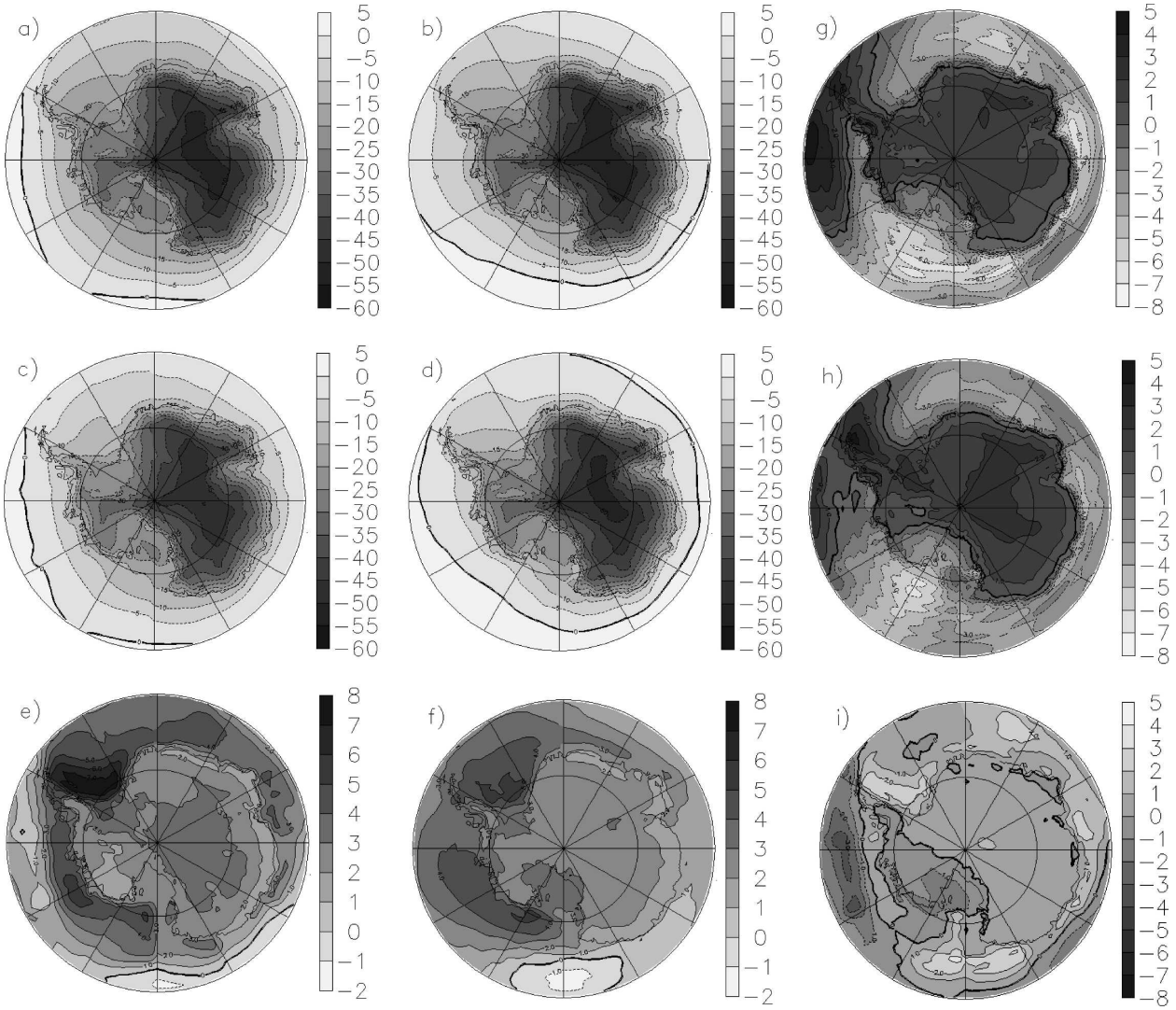

FIG. 7. As in Fig. 2, but for simulated surface air temperature (°C).

values in the interior and on the large ice shelves, net ablation in the Dry Valley area, generally strong gradients in the coastal regions, and high surface mass balances over the peninsula, particularly on the western side, and in Mary Byrd Land.

4. Simulated climate change

a. Temperature change

The simulated continental mean annual mean surface air temperature change is 2.8°C for A21–O20 and 2.6°C for S21–S20. The value is thus very similar on the continental scale, but regional differences exist. Figure 7 displays the annual mean surface air temperature for the simulations O20 (Fig. 7a), S20 (Fig. 7b), A21 (Fig. 7c), and S21(Fig. 7d); the simulated annual mean temperature changes A21–O20 (Fig. 7e) and S21–S20 (Fig. 7f); and the temperature change induced by the use of the anomaly method (O20–S20: Fig. 7g and A21–S21: Fig. 7h). Furthermore, Fig. 7i displays the difference of the effect of the anomaly method between the two periods considered [(A21–S21) − (O20–S20)]. In central East Antarctica, the temperature change simulated using the anomaly method (Fig. 7e) is stronger than the one simulated when the coupled model SSC are directly used (Fig. 7f). On the contrary, the warming with the anomaly method is weaker in West Antarctica, in particular in Mary Byrd Land. The weaker warming in this region is linked to atmospheric circulation changes in the Amundsen–Bellingshausen Seas area, which is in turn linked to the prescribed sea ice concentration

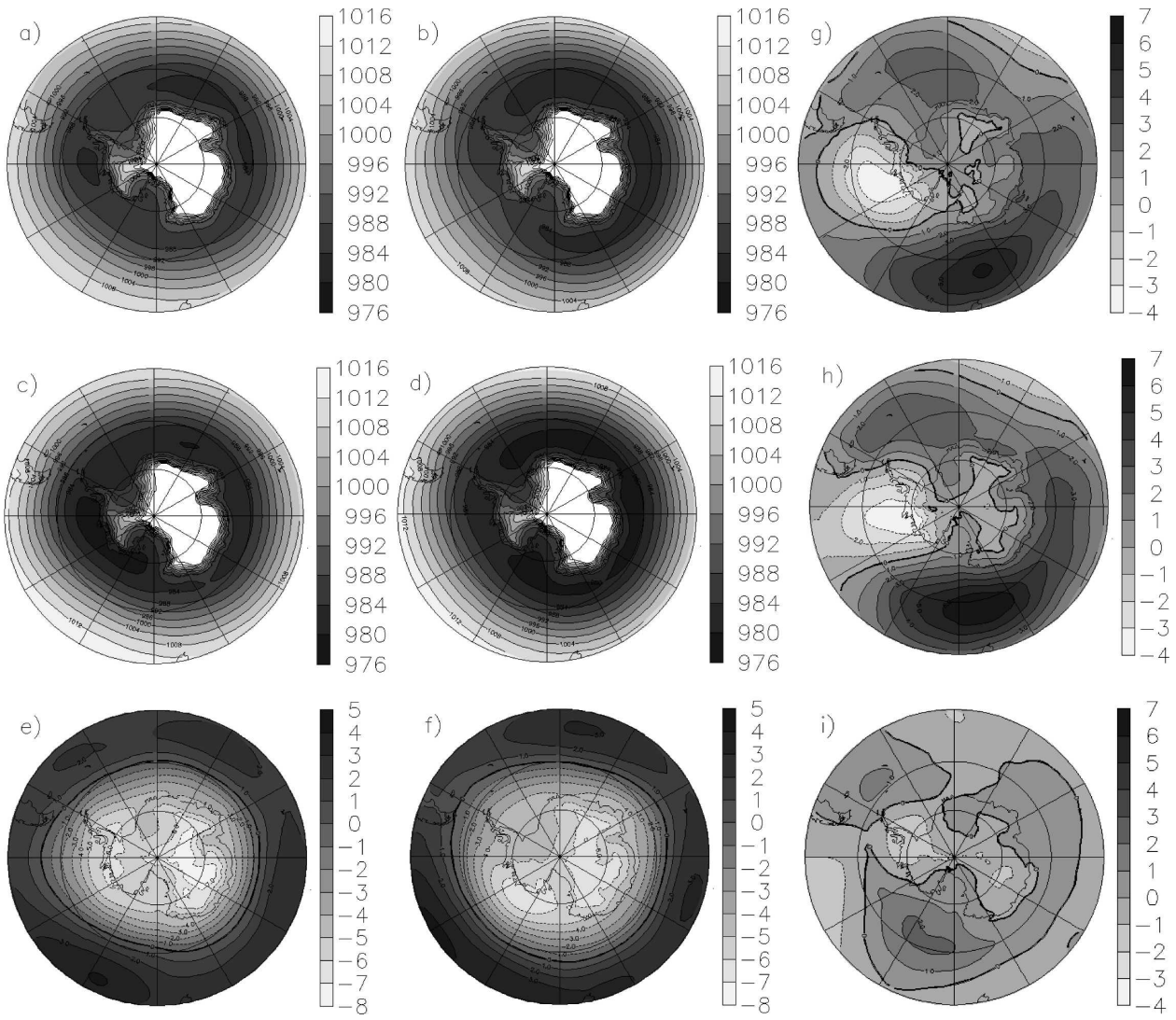

FIG. 8. As in Fig. 2, but for simulated annual sea level pressure (hPa).

changes. The prescribed sea ice concentration changes in that region (Figs. 2e,f) are such that the anomaly method yields the maximum sea ice concentration decrease farther east. Because of the strong link between Antarctic sea ice concentration and cyclonic activity (Simmonds and Wu 1993), this induces differential changes in cyclone density and thus sea level pressure (Fig. 8): the spatial patterns of sea level pressure changes in the Amundsen–Bellingshausen Seas area are very similar to the sea ice concentration changes. Over Mary Byrd Land, the modified sea level pressure patterns induce an increased cold outflow from the interior of the continent in A21 compared to O20 (Fig. 8e), thus weakening the future climate warming there (Fig. 7e). In S21 compared to S20, the sea level pressure changes do not induce such a cold flow (Fig. 8f), and therefore the future warming is not weakened (Fig. 7f). As stated before, the anomaly method yields a stronger warming in the interior of the continent. This might be linked to the fact that the prescribed absolute total change of sea ice extent from the end of the twentieth to the end of the twenty-first century is stronger with the anomaly method (Figs. 2e,f), because the IPSL CM4 coupled model simulates too little sea ice at all seasons (Fig. 1). Thus the change in oceanic energy available to heat the interior of the Antarctic continent is larger with the anomaly method, leading to a generally stronger climate change signal (except in regions such as Mary Byrd Land where regional circulation changes induce an opposite signal).

It is interesting to note that the impact of the

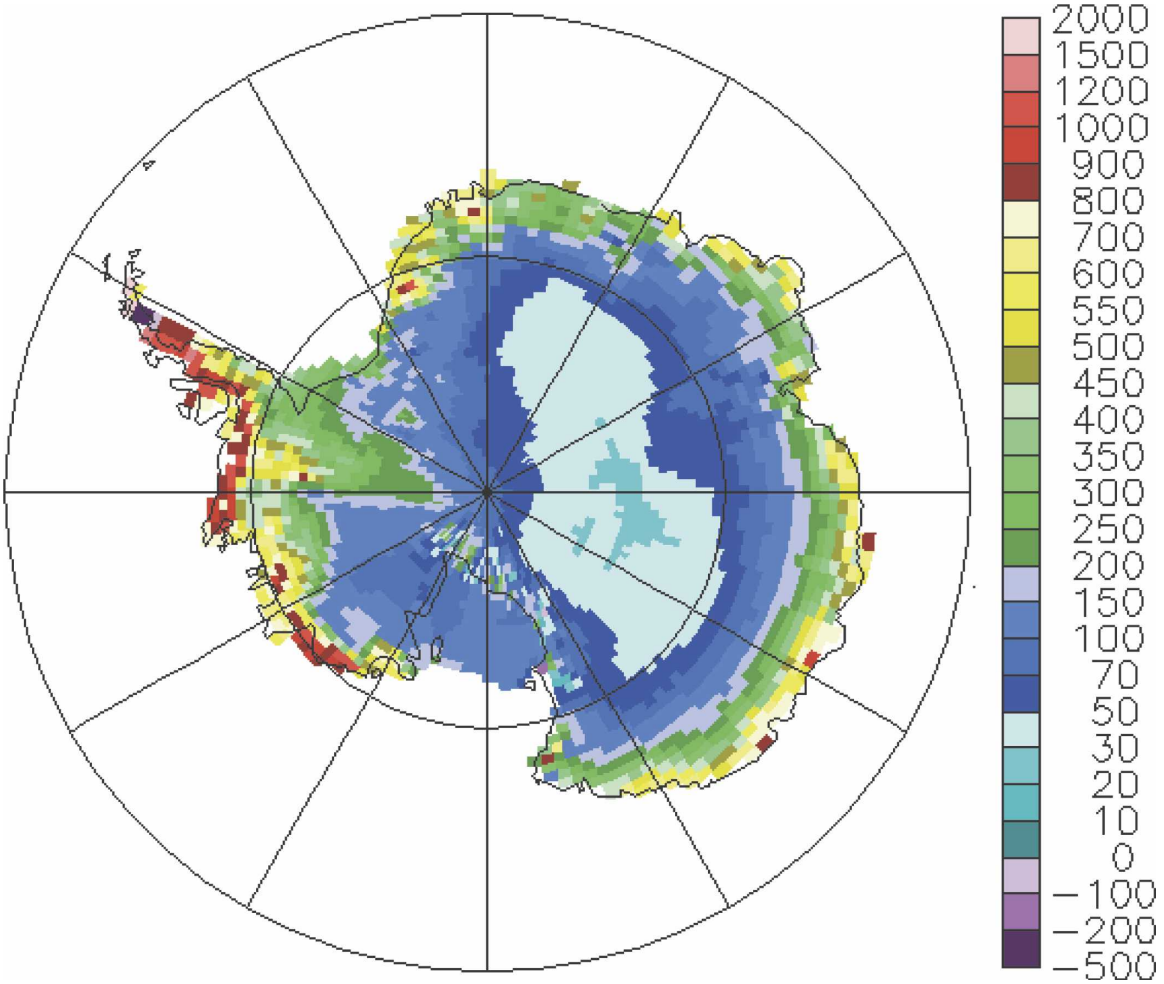

FIG. 9. Surface mass balance (kg m^{-2} yr^{-1}) simulated in A21 for 2081–2100, SRES A1B scenario.

anomaly method on the simulated annual mean surface air temperature is very similar for the end of the twentieth century (Fig. 7g) and the end of the twenty-first century (Fig. 7h). The difference between these two, shown in Fig. 7i, is indeed fairly weak. This is clearly linked to the similarity of the sea ice changes induced by the anomaly method at both periods (Figs. 2g,h). In the anomaly experiments O20 and A21, surface air temperatures over the oceans are reduced where the corrected sea ice concentration is higher than simulated by the coupled model, and vice versa. The same observation (similar impact of the anomaly method at both periods) applies to sea level pressure, as can be seen by visually comparing Figs. 8g and 8h. Again, the impact of the sea ice correction in the present-day simulation can be used as an excellent predictor of the impact of the anomaly method in the climate change experiment, at least as far as the spatial pattern of this impact is concerned.

b. *Surface mass balance change*

The continental mean surface mass balance (Fig. 9) is 204 kg m^{-2} yr^{-1} in A21, that is, 44 kg m^{-2} yr^{-1} more than in O20. The corresponding numbers for the grounded parts of the ice sheet are 153 kg m^{-2} yr^{-1} for O20 and 196 kg m^{-2} yr^{-1} for A21. This surface mass balance increase corresponds to a global eustatic sea level decrease of 1.5 mm yr^{-1}. This is about 40% more than the 1.05 mm yr^{-1} for the corresponding change between S20 and S21.[1] In both cases (A21 with respect to O20 and S21 with respect to S20), the surface mass balance increase from the end of the twentieth to the end of the twenty-first century is very similar to the precipitation increase, because the sublimation and

[1] Krinner et al. (2007) report 1.2 mm yr^{-1} for the difference between S21 and S20. This slightly different number resulted from an error in the grounded ice sheet mask they used.

TABLE 1. Regional precipitation changes ΔP ($\times 10^{12}$ kg yr^{-1}) from O20 to A21 and from S20 to S21. Here the limits between East and West Antarctica are the 180° and 30°W meridians.

Region	ΔP, A21−O20	ΔP, S21–S20
Antarctica	652	479
East Antarctica, coastal regions (below 1500 m)	140	86
West Antarctica, coastal regions (below 1500 m)	280	229
East Antarctica, intermediate altitudes (between 1500 and 2500 m)	95	55
West Antarctica, intermediate altitudes (between 1500 and 2500 m)	52	47
Plateau regions (above 2500 m)	85	61

runoff increases are each only of the order of 2 kg m^{-2} yr^{-1} and thus very small compared to the precipitation changes. Interannual variability of the continental mean SMB is 7 kg m^{-2} yr^{-1} in O20 and 9 kg m^{-2} yr^{-1} in A21.

Table 1 gives a breakdown of the precipitation changes between East and West Antarctica for different altitude bands. The spatially integrated precipitation increase is 652×10^{12} kg yr^{-1} in A21–O20 and 479×10^{12} kg yr^{-1} in S21–S20. Similar to what Krinner et al. (2007) already stated for S21–S20, the spatially integrated precipitation increase over the grid points below 1500 m is twice that over the grid points above 1500 m when the anomaly method is used. More than 40% of the total Antarctic precipitation increase occurs over the West Antarctic coastal regions in both climate change experiments. Figure 10 displays the precipitation and its changes for the different experiments. The strong precipitation increase over the Antarctic Peninsula (Figs. 10e,f) is consistent with the sea level pressure changes (Figs. 8e,f), which show increased westerly flow in this area, implying enhanced moisture advection from the Bellingshausen Sea, particularly in the anomaly experiment. Similarly, the precipitation reduction over the interior of Mary Byrd Land and the Ross Ice Shelf in the anomaly experiment is consistent with the increased outflow of cold, dry air from the interior of West Antarctica, which, as shown before, follows the sea level pressure changes induced by the sea ice concentration changes (Figs. 2e, 7e, and 8e). In coastal East Antarctica, the precipitation increase from O20 to A21 is fairly evenly distributed both in time (seasonally) and in space (longitudinally). It appears to be a fairly direct consequence of warming (linked to the imposed sea ice concentration decrease and greenhouse gas concentration increase) and increased cyclone intensity, as can be seen from the sea level pressure decrease (which, again, is linked to the imposed sea ice concentration decrease).

In this respect, it is noteworthy that the changes in cyclone system density and depth between O20 and A21 (not shown) are very similar to those reported by Krinner et al. (2007) for the changes between S20 and S21: system density increases off West Antarctica and decreases slightly off East Antarctica, the latter decrease being more than compensated for by an increase in the average intensity of the individual cyclonic systems, coherent with the sea level pressure decrease in the Antarctic region seen in Figs. 8e and 8f. In both experiments, the large-scale sea level pressure decrease in the Antarctic region is counterbalanced by a pressure increase at lower latitudes. This combined signal is equivalent to a more positive phase of the southern annular mode, as seen in previous climate change experiments (see Krinner et al. 2007, and references therein).

As already noted for temperature and surface air pressure, Figs. 10g and 10h illustrate that the precipitation change induced by the use of the anomaly method is very similar for both climatic periods considered. This is an obvious consequence of the fact that the precipitation changes are a consequence of the combined influences of circulation and temperature changes, which are similar for both periods. Thus, similar to what has been seen for temperature and sea level pressure, the impact of the anomaly scheme on the simulated precipitation (and hence surface mass balance) in the twentieth-century control experiments can be used as a predictor of its impact on the climate predictions. However, Fig. 10i shows that the anomaly method modifies the amplitude of some characteristics of the simulated climate change. For example, the projected dipole of precipitation change in West Antarctica (precipitation increase over the Antarctic Peninsula versus a decrease in parts of Mary Byrd Land; Figs. 10e,f) is amplified due to the impact of the anomaly method on the atmospheric circulation patterns (Figs. 8g,h).

As can be seen in Table 1, approximately 60% of the total difference of the spatially integrated precipitation increase between A21–O20 on one hand and S21–S20 on the other hand (105×10^{12} kg yr^{-1} out of 173×10^{12} kg yr^{-1}) occurs in the coastal regions below 1500-m altitude and this is about equally distributed between West and East Antarctica. Figure 10i displays the difference of the precipitation increase between A21–O20 on one hand and S21–S20 on the other hand. Large differences are visible in West Antarctica, where a di-

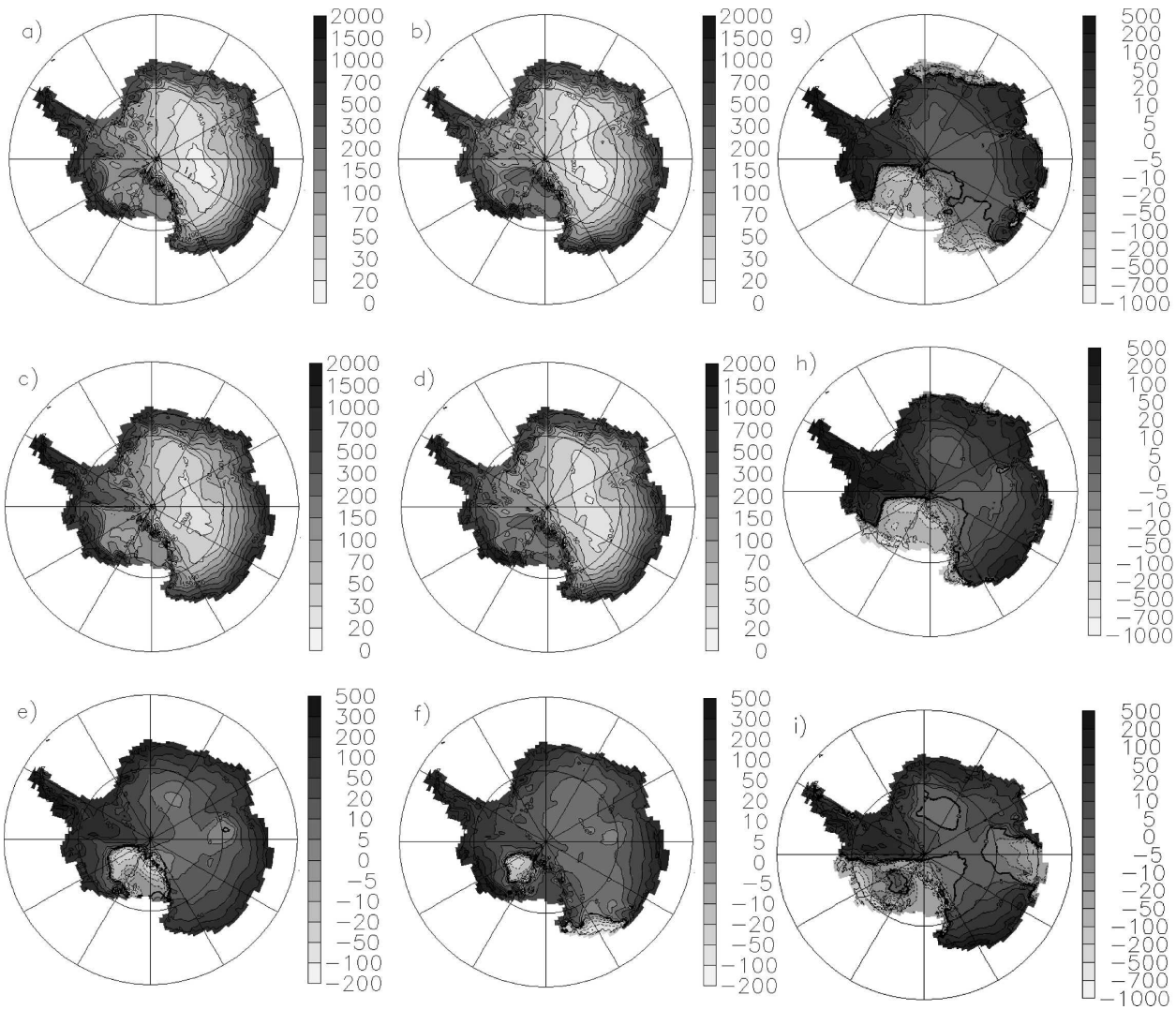

FIG. 10. As in Fig. 2, but for simulated annual mean precipitation (kg m^{-2} yr^{-1}).

pole exists between Mary Byrd Land and the Antarctic Peninsula (a consequence of sea level pressure changes linked to the prescribed sea ice changes, as shown before), and off Wilkes Land, where the anomaly method yields precipitation increase from O20 to A21, while the direct use of the coupled model SSC induces a precipitation decrease from S20 to S21, as discussed by Krinner et al. (2007). In both experiments, sea ice concentration changes in the next 100 yr off Wilkes Land are weak; there is even a slight increase, weaker in the anomaly experiment than in the original coupled model output. In this region, this slight difference is obviously enough to induce opposite precipitation changes coherent with the differences in the prescribed sea ice changes (more sea ice leading to cooler temperatures and thus a precipitation reduction).

c. *Atmospheric interannual variability and its link to sea ice*

As stated in section 2, our present-day simulation (O20) uses observed interannually varying SSC, but the prescribed interannual variability of SSC in the future simulation (A21) is derived from that of the coupled model. The question is: Does the way SSC are prescribed influence the simulated interannual Antarctic climate variability, and if yes, to what degree? Because we are principally interested in the simulated surface mass balance, and because precipitation is the dominant term of the simulated surface mass balance, we will in particular analyze the simulated interannual variability of precipitation. The first part of the question ("Does the way SSC are prescribed influence the

simulated interannual Antarctic climate variability?") is best answered by comparing the simulated climate variability in simulations with and without interannually varying SSC. Because we are interested in the impact of the anomaly method, the following analysis will focus on the simulations A21 (anomaly method, interannually varying SSC) and S21 (direct method, no interannually varying SSC).

Krinner et al. (2007) have shown that precipitation changes can be understood as a consequence of changes in temperature and atmospheric circulation patterns. We will therefore first analyze the interannual variability of the 500-hPa geopotential height (g500) and surface air temperature. Figure 11 displays the leading empirical orthogonal function (EOF) eigenvectors of g500 in A21 and S21, calculated using a 12-month moving average filter in order to remove the annual cycle. The first the EOFs explain 57%, 13%, and 7% of the simulated interannual variance in A21 and 60%, 10%, and 7% in S21. Similar to observations, the dominant mode of interannual variability in both simulations (Figs. 11a,d) is the well-known southern annular mode, which has been reported in previous studies to exist in both present and future climate simulations (Fyfe et al. 1999; Kushner et al. 2001; Stone et al. 2001; Cai et al. 2003; Marshall et al. 2004). This mode of variability seems to be fairly independent of oceanic forcing; rather, it is this type of internal atmospheric variability that has been reported to induce oceanic interannual variability (Hall and Visbeck 2002). The following modes of the g500 variability are also very similar in A21 and S21. These modes are characterized by centers of action in the Pacific and Atlantic sectors of the Southern Ocean. Antiphase relationships between these sectors of the Southern Ocean are characteristic of the Antarctic dipole (Yuan and Martinson 2000). These two modes have also previously been reported in atmospheric reanalyses (Genthon et al. 2003). As all three modes appear with similar weights in both simulations, that is, independent of whether interannually varying SSC are prescribed or not, they are internal modes of the atmosphere, at least in the LMDZ AGCM.

Figure 12 displays the leading EOF eigenvectors of the surface air temperature in A21 and S21, again calculated using a 12-month moving average filter in order to remove the annual cycle. The first EOFs explain 53%, 10%, and 8% of the simulated interannual variance in A21 and 58%, 14%, and 6% in S21. In both simulations the first EOF eigenvector (Figs. 12a,d) of the surface air temperature is clearly linked to the first EOF eigenvector of g500 (Figs. 11a,d): The time series of the EOF of these two variables are well correlated (r^2 = 77% for A21 and r^2 = 64% for S21, statistical significance >99%) and the temperature response pattern—opposite temperature variations between Mary Byrd Land and partially the peninsula on one hand and the rest of the continent on the other hand—is typical of the temperature variability induced by the southern annular mode (Thompson and Solomon 2002). One difference between the surface air temperature EOF eigenvectors of A21 and those of S21 is that, because the prescribed SSC contain no interannual variability in S21, the EOF eigenvectors of S21 show negligible variability over ice-free oceanic regions. Keeping this in mind and focusing on Antarctica (the continent and the sea-ice-covered ocean), one can associate the surface air temperature EOF2 of A21 with EOF3 of S21 (Figs. 12b,f) and vice versa (Figs. 12c,e). The first of these two variability patterns exhibits a center of action over the Weddell Sea, while the second is concentrated over Mary Byrd Land. Because the variance explained by the higher (>1) EOF modes both of surface air temperature and g500 is fairly low in both simulations (less than 15%), it is not surprising that the cross correlations between the time series of these higher EOF modes are not very clear for both simulations: r^2 does not reach 40% for any association between the higher modes of surface air temperature and g500 variability. Similar to what we have seen for g500, interannual SSC variability does not seem to influence in any particular way the spatial patterns of Antarctic surface temperature variability simulated by LMDZ.

Figure 13 displays the leading EOF eigenvectors of the normalized precipitation in A21 and S21. Normalized precipitation is defined as the 12-month running average filtered precipitation divided by the long-term mean simulated precipitation at each grid point. The first EOFs explain 19%, 15%, and 7% of the simulated interannual variance in A21 and 17%, 10%, and 9% in S21. This is considerably less than the variance of g500 and surface air temperature explained by the first EOF modes. This agrees with results reported by Genthon et al. (2003) who note that precipitation EOF are rather noisy and that it takes more leading precipitation EOF to explain a given fraction of the total variance than it does for other atmospheric fields. The spatial patterns of the normalized precipitation EOF eigenvectors of A21 (Figs. 13a–c) are very similar to, and in the same order as, the corresponding EOF eigenvectors of S21 (Figs. 13d–f). The first EOF eigenvector of normalized precipitation (Figs. 13a,d) is characterized by a dipole between the Pacific and Atlantic sectors of West Antarctica. This is physically coherent with the characteristics of the first surface air temperature EOF eigenvector (Figs. 12a,d), opposite temperature variations inducing opposite changes in the atmospheric moisture-

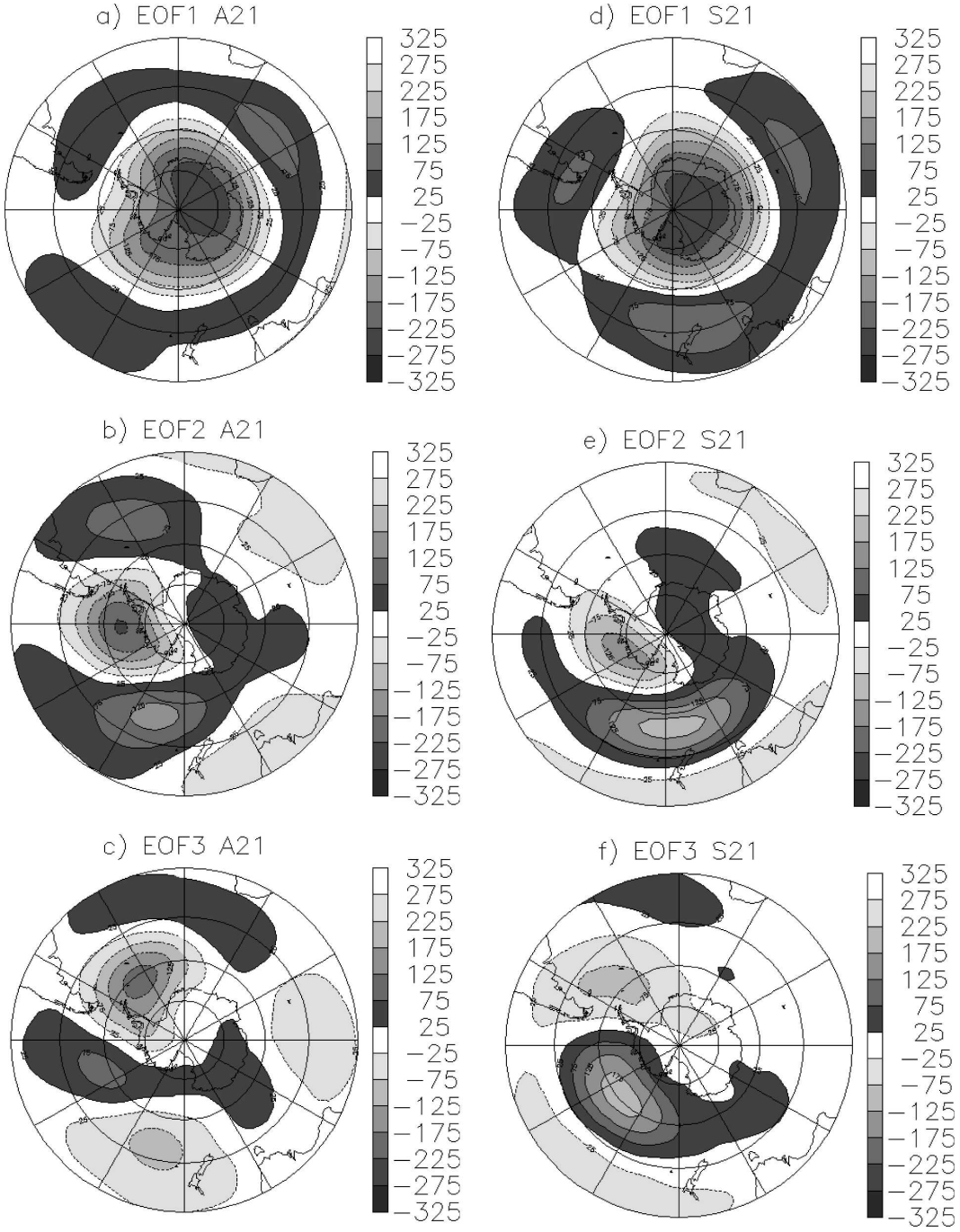

FIG. 11. Leading EOF eigenvectors of the 500-hPa geopotential height in simulations A21 and S21. (a) EOF1, A21; (b) EOF2, A21; (c) EOF3, A21; (d) EOF1, S21; (e) EOF2, S21; and (f) EOF3, S21.

holding capacity. This is supported, but not unequivocally confirmed, by the correlation of the time series of the respective EOFs. For A21 (S21), the first EOFs of surface air temperature and normalized precipitation correlate with $r^2 = 33\%$ (40%). In any case, the similarity of the normalized precipitation EOF of simulation A21 (Figs. 13a–c) with those of S21 (Figs. 13d–f), and the similar fractions of the total normalized precipitation variance explained by each of the modes in both simulations, clearly suggests that the normalized precipitation variability is similar in both simulations and fairly independent of any forcing by oceanic variability.

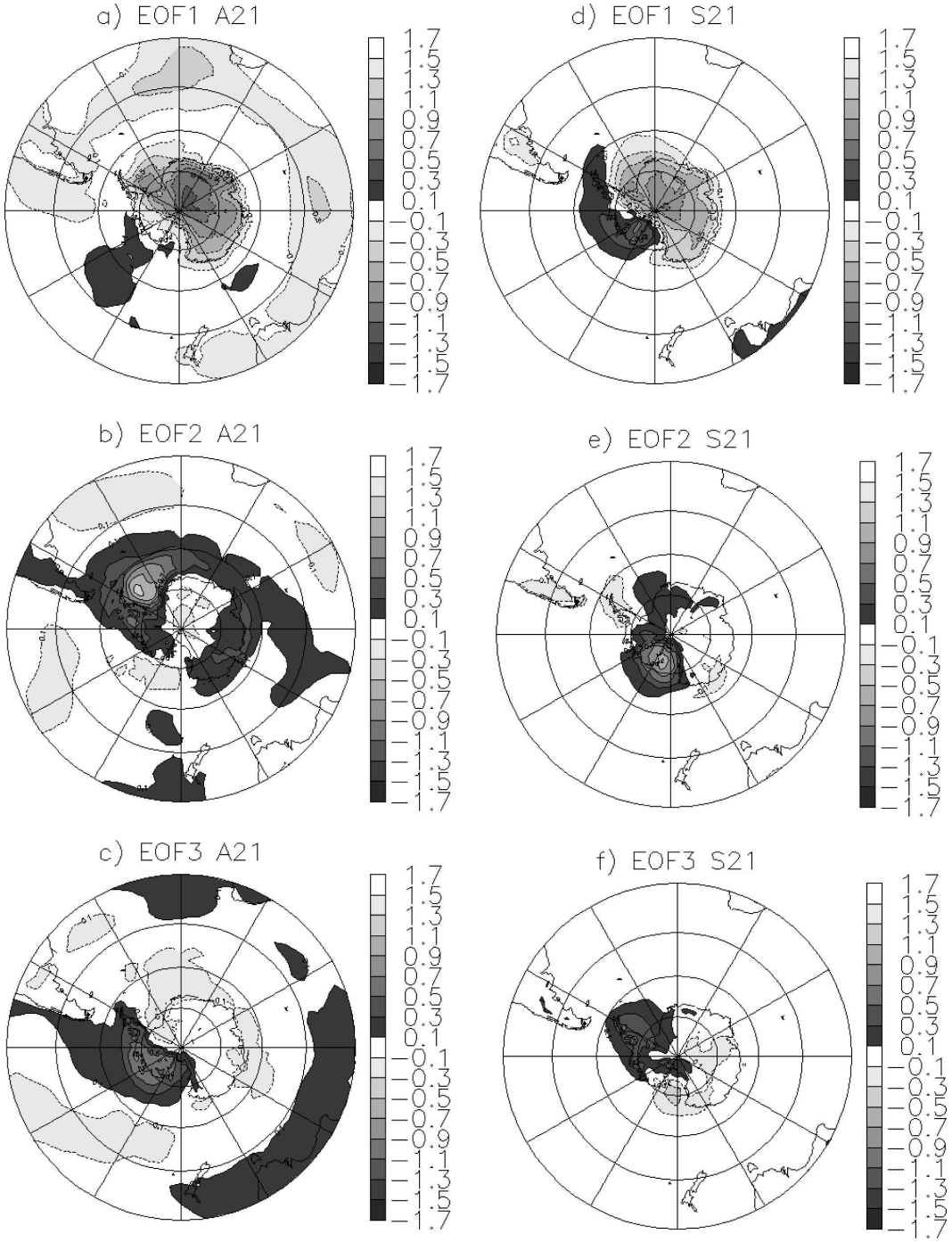

FIG. 12. Leading EOF eigenvectors of the surface air temperature in simulations A21 and S21. (a) EOF1, A21; (b) EOF2, A21; (c) EOF3, A21; (d) EOF1, S21; (e) EOF2, S21; and (f) EOF3, S21.

5. Discussion

The following discussion will focus on the simulated surface mass balance and its changes. The first question one might ask is: How do the mass balance changes simulated here compare with those of the IPCC Fourth Assessment Report coupled model runs? To address this question, we selected eight IPCC models based on their mean surface mass balance skill (see section 3c). For the IPCC models, we simply define the surface

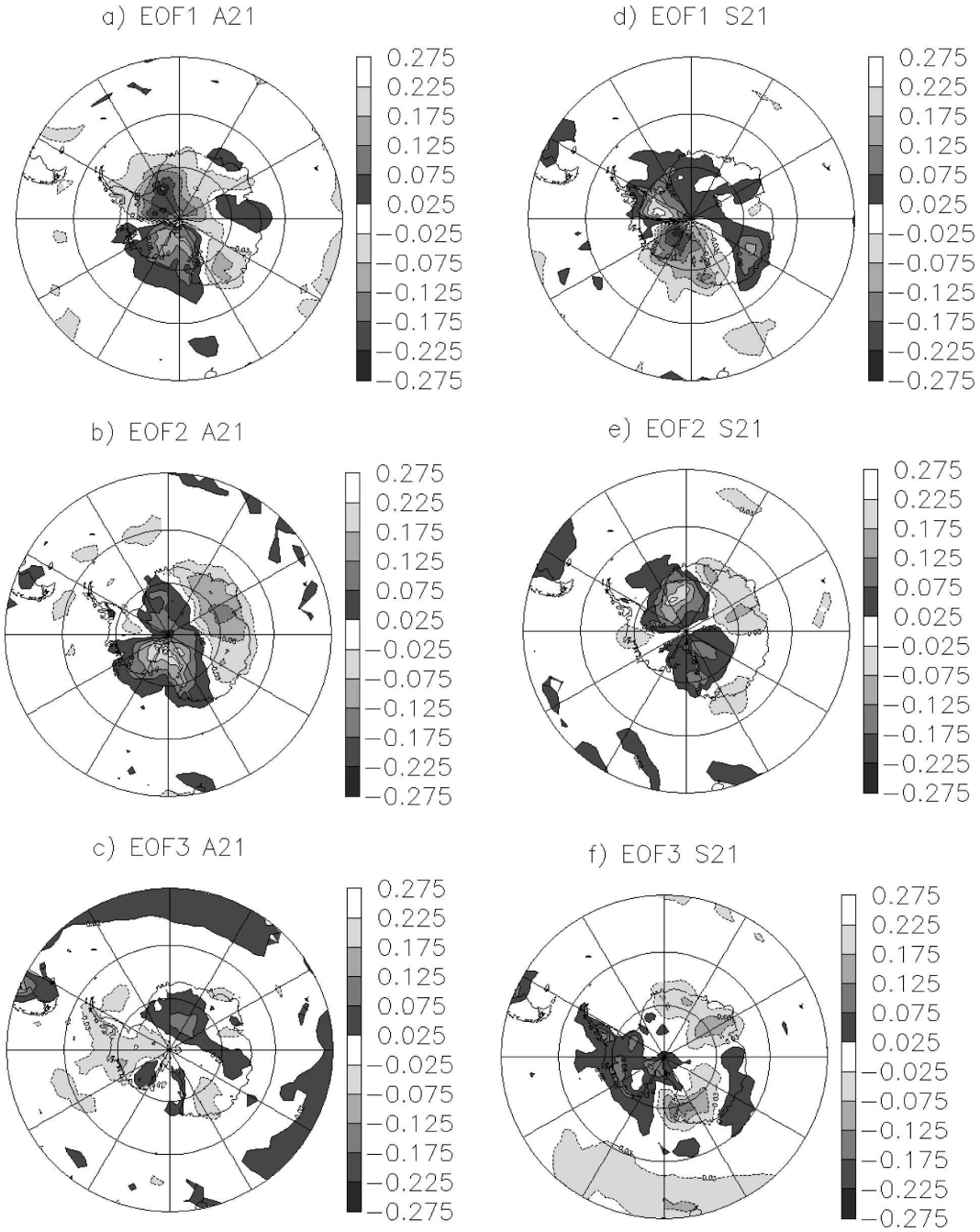

FIG. 13. Leading EOF eigenvectors of normalized precipitation (12-month moving average precipitation divided by the long-term mean) in simulations A21 and S21. (a) EOF1, A21; (b) EOF2, A21; (c) EOF3, A21; (d) EOF1, S21; (e) EOF2, S21; and (f) EOF3, S21.

mass balance as the difference between precipitation and sublimation/deposition, thereby neglecting surface melt, which is not easily diagnosed from the model output. As shown before, Antarctic mass loss by surface melt is likely to be minor even at the end of the twenty-first century, so this simplification will not significantly influence our results. Fixing the minimum skill for a model to be included in this analysis to a value of 0.7 leaves us with 8 models out of 20 (the skill varies from 0.28 to 0.76 for the 20 different models). Table 2 lists the continental mean surface mass balance for the two periods and the relative change within the 100 yr for

TABLE 2. Simulated Antarctic surface mass balance of selected IPCC Fourth Assessment Report coupled climate models. SMB skill: Surface mass balance skill (no unit, between 0 and 1); SMB: Continental mean surface mass balance (here defined as precipitation minus evaporation, in kg m^{-2} yr^{-1}) for 1981 to 2000 (20CM3 run) and 2081 to 2100 (SRES A1B run), and its relative change between these periods (in %).

Model	SMB skill	SMB 1981–2000 (kg m^{-2} yr^{-1})	SMB 2081–2100 (kg m^{-2} yr^{-1})	Relative change (from 1981–2000 to 2081–2100)
CCMA CGM3 T63	0.76	152	202	+33%
UKMO HADCM3	0.74	170	192	+13%
MIROC3 T106	0.73	184	248	+35%
MPI* ECHAM5	0.73	179	206	+15%
NCAR CCSM3**	0.72	200	238	+19%
UKMO HADGEM1	0.72	154	197	+28%
CCCMA CGM3 T47	0.71	182	218	+20%
IPSL CM4	0.71	156	173	+11%

* Max Planck Institute.
** National Center for Atmospheric Research Community Climate System Model, version 3.

these models. The mean relative surface mass balance change in 100 yr for these models is (+22 ± 9)%. With LMDZ4, we obtained a relative SMB increase of 28% with the anomaly method (O20 and S21) and a relative increase of 21% when the IPSL CM4 SSC were directly used (S20 and S21). The results obtained here are therefore in the range the intermodel dispersion of the IPPC runs, and the difference between the two numerical experiments using LMDZ4 (28% − 21% = 7%) is of the order of the IPCC intermodel dispersion (9%). That is, the way the oceanic boundary conditions are prescribed in regional downscaling experiments appears to be of similar importance as the choice of the model itself. The impact of the choice of the SSC and their implementation is in any case stronger than the typical dispersion among the members of IPCC ensemble runs with a given model, which is about 2%.

The choice between the "direct" use of the coupled model SSC and an anomaly method is therefore an important one. Both methods have their advantages and disadvantages. The bias of the present-day sea ice extent around Antarctica as simulated by IPSL CM4 is of the same magnitude as the sea ice extent difference between the end of the twentieth and the end of the twenty-first centuries (see Fig. 1). The present-day biases are thus far from being negligible compared to the projected climate change, even though the IPSL CM4 model does a comparably fair job in representing the present-day Antarctic climate. The simulated response of the system as a whole or one of its parts (here, the Antarctic surface climate) to a given forcing will, to some extent, depend on the baseline state, which in this case is partly determined by the imposed present-day sea ice conditions. However, our results (Figs. 7e,f, 8e,f, and 10e,f) show that the patterns of the simulated climate change (more specifically, surface air temperature, sea level pressure, and precipitation changes) are similar with both types of SSC. In other words, the patterns of simulated climate change appear fairly robust to "arbitrary" changes in the SSC, while the amplitude of the simulated climate change (and, in particular, precipitation change) does exhibit some sensitivity to the method used to prescribe the SSC in our experiments. This is similar to results obtained by Sushama et al. (2006), who used two versions of a regional climate model and report that the spatial patterns of the climate change signals in the two versions are regionally consistent, but the signals differ in magnitude.

Why is the continental mean precipitation change, and thus the projected impact on global sea level, stronger when the anomaly method is used? Figure 14, which displays the ratios between annual mean precipitation rates in different simulations, allows understanding this fairly easily. Figure 14a shows that, compared to the simulation that uses the coupled model's present-day SSC, the use of observed SSC induces a clear precipitation increase over the Antarctic Peninsula and the Filchner–Ronne Ice Shelf, and a decrease over Mary Byrd Land, the Ross Ice Shelf, and parts of Victoria Land, as discussed before. Figures 14b and 14c show that both climate change experiments exhibit a similar pattern of precipitation changes between the end of the twenty-first and the end of the twentieth century: a precipitation increase over the Antarctic Peninsula and the Filchner–Ronne Ice Shelf on one hand and a decrease over Mary Byrd Land and the Ross Ice Shelf or Victoria Land on the other hand. As a consequence of the difference in the twentieth century precipitation patterns, the simulated continental mean precipitation change in the anomaly experiment is stronger, because

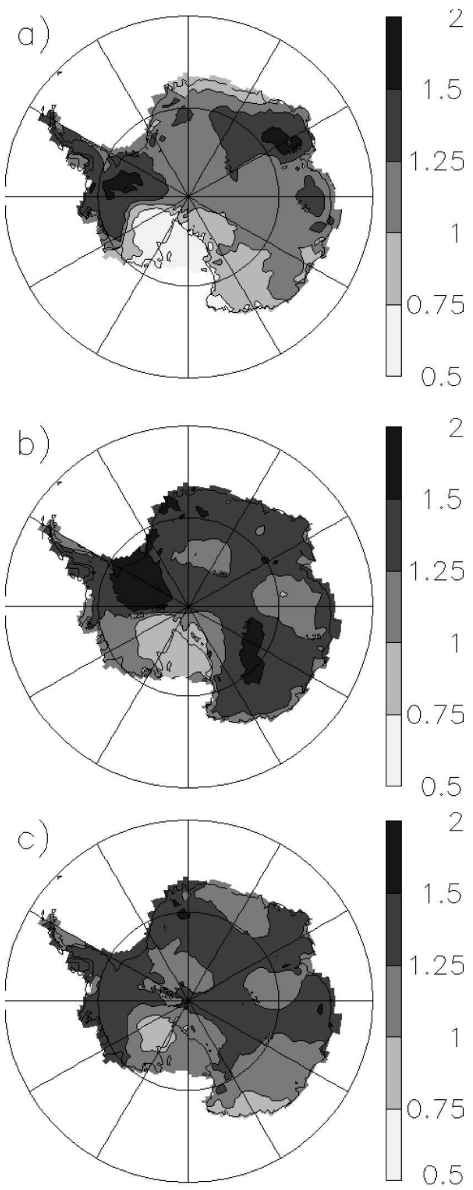

FIG. 14. Ratios of annual mean precipitation between different simulations: (a) O20/S20; (b) A21/O20; and (c) S21/S20.

the absolute precipitation increase over the Peninsula/Filchner–Ronne Ice Shelf region (Figs. 14b,c) is much stronger than in the experiment using "direct" SSC, and, similarly, the absolute precipitation decrease over Mary Byrd Land and Ross Ice Shelf or Victoria Land (same figures) is stronger in the climate change experiment using the "direct" SSC. Moreover, the mean temperature increase over East Antarctica is slightly stronger in the anomaly experiment (A21–O20) than in the "direct" SSC experiment (S21–S20), as can be seen in Figs. 7e, 7f, and 7i (see section 4a). Because of the link between temperature and moisture-holding capacity of air, this also leads to a stronger precipitation increase in the anomaly experiment. As stated in section 4a, the stronger temperature change over East Antarctica in the anomaly experiment might be linked to the fact that in this experiment, the continental-scale absolute sea ice concentration decrease is stronger than in the "direct" SSC experiment.

The patterns of the changes induced by using the anomaly method (instead of directly taking the SSC from the coupled model) are very similar for both climatic periods considered here, as shown before (Figs. 7g,h, 8g,h, and 10g,h), in spite of the nonlinear nature of the climate system. In other words, the impact of the corrected "anomaly" SSC (with respect to "direct" SSC from the coupled model) on the future climate is fairly well predictable when the impact of observed SSC (with respect to "direct" SSC from the coupled model) is known for the present-day control simulation. Moreover, the impact of the anomaly method on the simulated climate is physically consistent with the modifications to the prescribed sea ice coverage that the anomaly method induces.

The analysis of the simulated climate (g500, surface air temperature, and normalized precipitation) variability in section 4c has shown that this variability is fairly independent of the prescribed oceanic boundary conditions. In particular, whether SSC with or without interannual variability are prescribed, or whether the "anomaly" or "direct" method is used to construct these SSC in the future climate simulations, does not have much impact on the characteristics of the simulated variability. This is coherent with previous findings that show that the Antarctic climate variability, in particular in West Antarctica where it is particularly strong, is primarily induced by the asymmetric topography of the continent (Lachlan-Cope et al. 2001), and further displays temporal characteristics that suggest decoupling from oceanic forcing (Connolley 1997). This does not exclude, however, that the West Antarctic climate variability modes might in some cases be paced by ENSO (e.g., Genthon and Cosme 2003; Fogt and Bromwich 2006), but this is not important in the type of application presented here.

Pan et al. (2001) state that a large ratio R between the simulated climate change signal Δ and the model bias B, $R = \Delta/B$, must be seen as a necessary, albeit not sufficient, condition for reliable climate change projection. They view this condition as "conservative in comparison with bias-cancellation assumptions conventionally used for interpretation of climate change" (Pan et al. 2001). For the "anomaly" climate change experiment (simulations O20 and A21), the average surface mass balance bias B at the locations where reliable SMB

measurements exist equals 23% (corresponding to the mean skill of 77% as reported in section 3c), while the mean precipitation change on the same locations amounts to $\Delta = 27\%$. This means that $R = 1.17$. For the climate change experiment using directly the coupled model SSC (experiments S20 and S21), the corresponding numbers are $B = 28\%$, $\Delta = 19\%$, and thus $R = 0.70$. In other words, the reduced SMB bias leads to an a priori more reliable climate change projection. It therefore seems desirable to eliminate the systematic errors of the simulated SSC in downscaling exercises by using an anomaly method to construct the future SSC.

The way an anomaly method is implemented necessarily contains some degrees of freedom. For example, the number of sectors (here, 12) could be increased in order to reproduce more finely smaller-scale features of the sea ice concentration change simulated by the coupled model. However, there is a limit to the fine-scale detail one should try to preserve. For example, if the coupled model simulates much sea ice for the present and a strong future sea ice concentration decrease in a small region where only little sea ice is actually present in the real world, the use of a high number of (small) longitudinal sectors will lead to distributing this change over the whole Antarctic region because the relative hemispheric sea ice concentration change must be reproduced; the small-scale signal then becomes totally smeared out. Increasing the size of the sectors guarantees that such signals are reproduced approximately in the region where they occur in the coupled model. In any case, both the aim to conserve several basic characteristics (spatial and temporal variability; relative change of sea ice extent rather than the absolute change) of the coupled model SSC change in the constructed SSC for the regional high-resolution simulations, and the need to prevent pathological cases such as negative sea ice concentrations, preclude the simple solution of explicitly adding the coupled model climate change anomalies to the present-day observations. The anomaly method presented here is designed to serve as an objective interpretation of the coupled model's climate change signal in the light of the spatial and temporal structure of the observed present-day SSC, and it is the simplest possible method compliant with the criteria enumerated in section 2.

In the present case, the use of the anomaly method increases the simulated continental-mean surface mass balance change by about 40%, while the continental mean, annual mean surface air temperature change is essentially not affected. This is interesting in several aspects. First, it highlights once more the fact the link between temperature and precipitation changes over the ice sheets is not always as trivial as the simple moisture-holding capacity argument (Robin 1977) suggests. Second, it shows that the surface mass balance, particularly in the coastal regions, is very sensitive to the oceanic boundary conditions (see Table 2). In particular, it is somewhat more sensitive than the surface air temperature. This also argues in favor of the use of high-resolution models to evaluate future Antarctic surface mass balance changes, because only high-resolution models adequately resolve the steep coastal orography of the ice sheets. As can be seen in Table 2, the medium-resolution (300 km) IPSL CM4 model only simulated a continental-mean centennial-scale SMB increase of about 11%, compared to the 21% or 28% simulated by its atmospheric component LMDZ4 at 60 km (simulations presented here). Similarly, high-resolution models of the current IPCC exercise such as Model for Interdisciplinary Research on Climate 3 (MIROC3) T106, Canadian Centre for Climate Modelling and Analysis (CCCma) Coupled General Circulation Model, version 3 (CGCM3) T63, and the Met Office (UKMO) Hadley Centre Global Environmental Model version 1 (HadGEM1) (192×145 grid points) also show stronger surface mass balance changes than their lower-resolution "relatives" MIROC3 T42, CCCma CGCM3 T47, and UKMO Third Hadley Centre Coupled Ocean–Atmosphere General Circulation Model (HadCM3) (96×73 grid points), as can be seen in Table 2 (MIROC3 T42, excluded from Table 2 because of its SMB skill of 0.63, suggests a mean Antarctic SMB increase of only 8% between the periods considered here).

6. Conclusions

This paper presents the results of high-resolution AGCM simulations of the Antarctic climate for the periods 1981 to 2000 and 2081 to 2100. As oceanic boundary conditions, we used observed SSC for the period 1981 to 2000. For the period 2081 to 2100, we used an anomaly method based on present-day observations and the climate change signal from an IPCC SRES A1B run.

Compared to the direct use of the coupled model sea surface conditions as oceanic boundary conditions for the regional downscaling experiment, the use of the anomaly method increases previous estimates of the impact of Antarctic surface mass balance changes on global eustatic sea level change (Krinner et al. 2007) by about 40%. The simulated surface mass balance changes of the grounded Antarctic ice sheet between the ends of the twentieth and the twenty-first centuries correspond to an eustatic sea level decrease of about 1.5 mm yr^{-1}. Supposing gradual and linear Antarctic SMB

changes over the next century, the total impact on global sea level over 100 yr would therefore amount to −7.5 cm. We point out that this number does not take into account any potential changes of glacier dynamics in Antarctica, which might be revealed to be of major importance (Zwally et al. 2002; de Angelis and Skvarca 2003; Rignot et al. 2004). The differences in the results obtained with the two methods can be explained in terms of modified circulation patterns in response to the different sea ice concentration changes, in particular in West Antarctica, where the ice sheet climate is very sensitive to the atmospheric circulation and sea ice conditions (Genthon et al. 2005). It is remarkable that the simulated atmospheric variability patterns are relatively independent of the prescribed SSC and the way the oceanic changes are prescribed ("anomaly" versus "direct" method), given that the simulated climate and climate change are very sensitive to these boundary conditions. This suggests that one need not be too concerned about the way future interannual SSC variability is prescribed when an anomaly method is used.

However, because the climate change signal we obtain depends on the present-day baseline climate, and the biases of present-day simulated sea ice extents are of the order of the expected change over the next century, we feel that using an anomaly method in the construction of future SSC (which allows the use of present-day observed SSC in the control simulation) can, in some cases, be preferable over directly using SSC from a coupled model climate change experiment. The superiority of the anomaly method cannot be proved until observed climate data exist for the end of the twenty-first century. However, following Pan et al. (2001), the confidence not only in the simulated future climate, but also in the simulated climate change, is increased by the fact that the ratio between the amplitude of the projected climate change and the model bias (in particular concerning surface mass balance) is increased by using an anomaly method.

Another argument for using an anomaly method for studying regional climate change is computational efficiency. Using an anomaly method, climate change signals from other coupled AOGCMs can be used in future climate simulations without having to carry out a new present-day control simulation for each future climate simulation. This would be necessary if the SSC from the coupled models were used with the "direct" method.

A stretched-grid GCM such as the one used in this work is the ideal tool for downscaling large-scale climate change simulations with the anomaly method. In the particular case here, the regional downscaling with the anomaly method can be carried out in a very consistent way because LMDZ4, the model used for the downscaling, is the atmospheric component of the IPSL CM4 coupled model, which delivered the SSC for the climate change experiment. SSC anomaly methods cannot be easily applied in regional climate models, because these are forced by a GCM at their lateral boundaries; to be more precise, applying the SSC anomaly method in a regional climate model (RCM) would require the forcing atmospheric GCM to be run first with the anomaly method using the oceanic climate change signal from a coupled model run—this would not be practical, add uncertainties, and induce additional numerical cost. The "absolute" method, on the other hand, can be used in a regional climate model, provided the corresponding atmospheric boundary conditions, typically at a 6-h time step, are saved during the coupled model climate change experiment.

Both the "direct" or an "anomaly" method are of interest, depending on the kind of application. The point of this paper is not to dismiss the use of the "direct" method. Rather, one of the main results of this work is that we have shown the importance of the method used to construct SSC in a downscaling exercise with a high-resolution atmospheric model. In terms of simulated future surface mass balance changes, the results obtained with the "direct" and the "anomaly" method in our AGCM differ as much as those obtained by using different coupled GCMs.

Finally, it is remarkable that there seems to exist a link between model resolution and the simulated future Antarctic surface mass balance change: higher-resolution models tend to simulate a stronger SMB increase, apparently because of a better representation of coastal precipitation changes. This should be kept in mind when IPCC model runs are used to estimate future sea level changes.

Acknowledgments. This work was financed by the French programs ACI C_3, ACI MC^2, and ANR IDEGLACE, and the European integrated project ENSEMBLES. The simulations were carried out on the Mirage computer platform in Grenoble. Additional computer resources at IDRIS are acknowledged. In Wilkes and Victoria Land sectors, most of observed SMB data were obtained from recent research carried out in the framework of the Project on Glaciology of the PNRA-MIUR and financially supported by PNRA consortium through collaboration with ENEA Roma, and supported by the French Polar Institute (IPEV). This last work is a French–Italian contribution to the ITASE Project.

REFERENCES

Armstrong, R., M. J. Brodzik, and A. Varani, 1997: The NSIDC EASE-Grid: Addressing the need for a common, flexible, mapping and gridding scheme. *Earth Syst. Monit.,* **7,** 6–14.

Arthern, R. J., D. P. Winebrenner, and D. G. Vaughan, 2006: Antarctic snow accumulation mapped using polarization of 4.3-cm wavelength microwave emission. *J. Geophys. Res.,* **111,** D06107, doi:10.1029/2004JD005667.

Cai, W., P. H. Whetton, and D. J. Karoly, 2003: The response of the Antarctic Oscillation to increasing and stabilized atmospheric CO_2. *J. Climate,* **16,** 1525–1538.

Charbit, S., C. Ritz, and G. Ramstein, 2002: Simulations of Northern Hemisphere ice-sheet retreat: Sensitivity to physical mechanisms involved during the last deglaciation. *Quat. Sci. Rev.,* **21,** 243–265.

Connolley, W. M., 1997: Variability in annual mean circulation in southern high latitudes. *Climate Dyn.,* **13,** 745–756.

Cuffey, K. M., G. D. Clow, R. B. Alley, M. Stuiver, E. D. Waddington, and R. W. Saltus, 1995: Large Arctic temperature change at the Wisconsin-Holocene glacial transition. *Science,* **270,** 455–458.

de Angelis, H., and P. Skvarca, 2003: Glacier surge after ice shelf collapse. *Science,* **299,** 1560–1562.

de F. Forster, P. M., and K. E. Taylor, 2006: Climate forcings and climate sensitivities diagnosed from coupled climate model integrations. *J. Climate,* **19,** 6181–6194.

de Noblet-Ducoudré, N., M. Claussen, and C. Prentice, 2000: Mid-Holocene greening of the Sahara: First results of the GAIM 6000 year BP experiment with two asynchronously coupled atmosphere/biome models. *Climate Dyn.,* **16,** 643–659.

EPICA Community Members, 2004: Eight glacial cycles from an Antarctic ice core. *Nature,* **429,** 623–628.

Fogt, R. L., and D. H. Bromwich, 2006: Decadal variability of the ENSO teleconnection to the high-latitude South Pacific governed by coupling with the southern annular mode. *J. Climate,* **19,** 979–997.

Frezzotti, M., and Coauthors, 2004: New estimations of precipitation and surface sublimation in East Antarctica from snow accumulation measurements. *Climate Dyn.,* **23,** 803–813.

——, and Coauthors, 2005: Spatial and temporal variability of snow accumulation in East Antarctica from traverse data. *J. Glaciol.,* **51,** 113–124.

Füssel, H.-M., and J. G. van Minnen, 2001: Climate impact response functions for terrestrial ecosystems. *Integr. Assess.,* **2,** 183–197.

Fyfe, J. C., G. J. Boer, and G. M. Flato, 1999: The Arctic and Antarctic Oscillations and their projected changes under global warming. *Geophys. Res. Lett.,* **26,** 1601–1604.

Gallée, H., G. Guyomarc'h, and E. Brun, 2001: Impact of snow drift on the Antarctic ice sheet surface mass balance: Possible sensitivity to snow-surface properties. *Bound.-Layer Meteor.,* **99,** 1–19.

Genthon, C., and E. Cosme, 2003: Intermittent signature of ENSO in west-Antarctic precipitation. *Geophys. Res. Lett.,* **30,** 2081, doi:10.1029/2003GL018280.

——, G. Krinner, and M. Sacchettini, 2003: Interannual Antarctic tropospheric circulation and precipitation variability. *Climate Dyn.,* **21,** 289–307.

——, S. Kaspari, and P. A. Mayewski, 2005: Interannual variability of the surface mass balance of West Antarctica from ITASE cores and ERA40 reanalyses, 1958–2000. *Climate Dyn.,* **24,** 759–770.

Gibson, R., P. Kållberg, and S. Uppala, 1996: The ECMWF re-analysis (ERA) project. *ECMWF Newsletter,* No. 73, ECMWF, Reading, United Kingdom, 7–17.

Giorgi, F., and L. O. Mearns, 1991: Approaches to the simulation of regional climate change: A review. *Rev. Geophys.,* **29,** 191–216.

Giovinetto, M. B., D. H. Bromwich, and G. Wendler, 1992: Atmospheric net transport of water vapor and latent heat across 70°S. *J. Geophys. Res.,* **97,** 917–930.

Hall, A., and M. Visbeck, 2002: Synchronous variability in the Southern Hemisphere atmosphere, sea ice, and ocean resulting from the annular mode. *J. Climate,* **15,** 3043–3057.

Hewitson, B., 2003: Developing perturbations for climate change impact assessments. *Eos, Trans. Amer. Geophys. Union,* **84,** 337–348.

Hourdin, F., and Coauthors, 2006: The LMDZ4 general circulation model: Climate performance and sensitivity to parametrized physics with emphasis on tropical convection. *Climate Dyn.,* **27,** 787–813.

Huybrechts, P., J. Gregory, I. Janssens, and M. Wild, 2004: Modelling Antarctic and Greenland volume changes during the 20th and 21st centuries forced by GCM time slice integrations. *Global Planet. Change,* **42,** 83–105.

Krinner, G., and C. Genthon, 1999: Altitude dependence of the ice sheet surface climate. *Geophys. Res. Lett.,* **26,** 2227–2230.

——, and M. Werner, 2003: Impact of precipitation seasonality changes on isotopic signals in polar ice cores: A multi-model analysis. *Earth Planet. Sci. Lett.,* **216,** 525–538.

——, C. Genthon, Z.-X. Li, and P. Le Van, 1997: Studies of the Antarctic climate with a stretched-grid general circulation model. *J. Geophys. Res.,* **102,** 13 731–13 746.

——, J. Mangerud, M. Jakobsson, M. Crucifix, C. Ritz, and J. I. Svendsen, 2004: Enhanced ice sheet growth in Eurasia owing to adjacent ice-dammed lakes. *Nature,* **427,** 429–432.

——, O. Magand, I. Simmonds, C. Genthon, and J.-L. Dufresne, 2007: Simulated Antarctic precipitation and surface mass balance at the end of the twentieth and twenty-first centuries. *Climate Dyn.,* **28,** 215–230.

Kushner, P. J., I. M. Held, and T. L. Delworth, 2001: Southern Hemisphere atmospheric circulation response to global warming. *J. Climate,* **14,** 2238–2249.

Lachlan-Cope, T. A., W. M. Connolley, and J. Turner, 2001: The role of the non-axisymmetric Antarctic orography in forcing the observed pattern of variability of the Antarctic climate. *Geophys. Res. Lett.,* **28,** 4111–4114.

Lunt, D. J., N. de Noblet-Ducoudré, and S. Charbit, 2004: Effects of a melted Greenland ice sheet on climate, vegetation, and the cryosphere. *Climate Dyn.,* **23,** 679–694.

Marshall, G. J., P. A. Stott, J. Turner, W. M. Connolley, J. C. King, and T. A. Lachlan-Cope, 2004: Causes of exceptional atmospheric circulation changes in the Southern Hemisphere. *Geophys. Res. Lett.,* **31,** L14205, doi:10.1029/2004GL019952.

Marti, O., and Coauthors, 2005: The new IPSL climate system model: IPSL-CM4. Note du Pôle de Modélisation 26, IPSL, 86 pp. [Available online at http://dods.ipsl.jussieu.fr/omamce/IPSLCM4/DocIPSLCM4/.]

Masson-Delmotte, V., and Coauthors, 2006: Past and future polar amplification of climate change: Climate model intercomparisons and ice-core constraints. *Climate Dyn.,* **27,** 437–440.

Pan, Z., J. H. Christensen, R. W. Arritt, W. J. Gutowski Jr., E. S. Takle, and F. Otieno, 2001: Evaluation of uncertainties in

regional climate change simulations. *J. Geophys. Res.,* **106,** 17 735–17 752.

Pfeffer, W. T., M. F. Meier, and T. H. Illangasekare, 1991: Retention of Greenland runoff by refreezing: Implications for projected future sea level change. *J. Geophys. Res.,* **96,** 22 117–22 124.

Rignot, E., G. Casassa, P. Gogineni, W. Krabill, A. Rivera, and R. Thomas, 2004: Accelerated ice discharge from the Antarctic Peninsula following the collapse of Larsen B ice shelf. *Geophys. Res. Lett.,* **31,** L18401, doi:10.1029/2004GL020697.

Robin, G., 1977: Ice cores and climatic change. *Philos. Trans. Roy. Soc. London,* **B280,** 143–168.

Santer, B., 1985: The use of general circulation models in climate impact analysis—A preliminary study of the impacts of a CO_2-induced climatic change on west European agriculture. *Climatic Change,* **7,** 71–93.

Simmonds, I., and W. F. Budd, 1991: Sensitivity of the Southern Hemisphere circulation to leads in the Antarctic pack ice. *Quart. J. Roy. Meteor. Soc.,* **117,** 1003–1024.

——, and X. Wu, 1993: Cyclone behaviour response to changes in winter Southern Hemisphere sea-ice concentration. *Quart. J. Roy. Meteor. Soc.,* **119,** 1121–1148.

Stone, D. A., A. J. Weaver, and R. J. Stouffer, 2001: Projection of climate change onto modes of atmospheric variability. *J. Climate,* **14,** 3551–3565.

Sushama, L., R. Laprise, D. Caya, A. Frigon, and M. Slivitzky, 2006: Canadian RCM projected climate-change signal and its sensitivity to model errors. *Int. J. Climatol.,* **26,** 2141–2159.

Thompson, D. W. J., and S. Solomon, 2002: Interpretation of recent Southern Hemisphere climate change. *Science,* **296,** 895–899.

Thompson, S. L., and D. Pollard, 1997: Greenland and Antarctic mass balances for present and doubled atmospheric CO_2 from the GENESIS version-2 global climate model. *J. Climate,* **10,** 871–900.

Wild, M., A. Ohmura, and U. Cubasch, 1997: GCM-simulated surface energy fluxes in climate change experiments. *J. Climate,* **10,** 3093–3110.

——, P. Calanca, S. C. Scherrer, and A. Ohmura, 2003: Effects of polar ice sheets on global sea level in high-resolution greenhouse scenarios. *J. Geophys. Res.,* **108,** 4165, doi:10.1029/2002JD002451.

Yamazaki, K., 1994: Moisture budget in the Antarctic atmosphere. *Snow and Ice Covers: Interactions with the Atmosphere and Ecosystems,* IAHS Publication 233, H. G. Jones et al., Eds., IAHS Press, 61–67.

Yuan, X., and D. G. Martinson, 2000: Antarctic sea ice extent variability and its global connectivity. *J. Climate,* **13,** 1697–1717.

Zwally, H. J., W. Abdalati, T. Herring, K. Larson, J. Saba, and K. Steffen, 2002: Surface melt-induced acceleration of Greenland ice-sheet flow. *Science,* **297,** 218–222.

——, M. B. Giovinetto, J. Li, H. G. Cornejo, M. A. Beckley, A. C. Brenner, J. L. Saba, and D. Yi, 2005: Mass changes of the Greenland and Antarctic ice sheets and shelves and contributions to sea-level rise: 1992–2002. *J. Glaciol.,* **51,** 509–527.